minerals

MDPI

Article

Geological and Geochemical Constraints on the Origin of the Sr Mineralization in Huayingshan Ore District, Chongqing, South China

Yun Gao [1,2], Yan Sun [2,*], Denghong Wang [2], Bailin Chen [3] and Wenshuai Gu [4]

[1] State Key Laboratory of Mineral Processing, BGRIMM Technology Group, Beijing 102628, China
[2] Institute of Mineral Resources, Chinese Academy of Geological Sciences, Beijing 100037, China
[3] Key Laboratory of Paleomagnetism and Tectonic Reconstruction, Institute of Geomechanics, Chinese Academy of Geological Sciences, Beijing 100081, China
[4] 205 Geological Team, Chongqing Bureau of Geology and Mineral Resources Exploration, Chongqing 402160, China
* Correspondence: sunyan@cags.ac.cn

Abstract: There are many celestine deposits and mineralization points in the Huayingshan ore district which form the largest strontium resource base in China. Among these celestine deposits, the Yuxia and Xinglong are two of the larger deposits. Previous studies have displayed different views on the genesis of the celestine deposit in the Huayingshan ore district. In this study, we conducted field obversions, geochemistry, and fluid inclusion studies to investigate the sources of ore-forming matters and the metallogenic mechanism of the celestine deposit. Four types of fluid inclusion (FI), namely PL (pure liquid FI), PV (pure vapor FI), L-V (liquid-vapor two-phase FI), and L-V-S (liquid-vapor-solid three-phase FI) have been identified in celestine from different types of ore in the Xishan anticline. The ore-forming fluids belong to the NaCl-H_2 O system with moderate to low temperature (190–220 °C) and moderate salinity (5–9 wt%, NaCl equiv.). Different types of ores were formed by the same period of hydrothermal activity, which is supported by the results of the microthermometer study. Geological, thermometric data, and published hydrogen and oxygen isotope results indicate that the hot brines associated with mineralization mainly originated from meteoric water and some of diagenetic fluid. The Sr ($^{87}Sr/^{86}Sr$ = 0.7076–0.7078) and S ($\delta^{34}S$ = 36.4–39.0) isotope values of celestine are consistent with those of the Jialingjiang Formation, indicating that ore metals in hot brines were predominantly derived from that formation. In situ analysis of celestine shows that there is a strong negative correlation between Sr and CaO (R^2 = 0.95) and combined with mineralogical and isotope geochemical evidence, we concluded that the precipitation mechanism of celestine is the replacement of gypsum with Sr-rich hot brines. Based on the above research and the classification of celestine deposit type, we classified the celestine deposits in Huayingshan as being of hydrothermal type. The formation of celestine deposits can be divided into three periods: (1) evaporation period, forming the source bed; (2) hydrothermal activity period, forming celestine by replacement of gypsum with Sr-rich hot brines; (3) supergene period, where meteoric water dissolves orebodies and strontianization occurs.

Keywords: celestine deposit; strontium isotope; sulfur isotope; fluid inclusion; Triassic; Huayingshan; Sichuan Basin

check for updates

Citation: Gao, Y.; Sun, Y.; Wang, D.; Chen, B.; Gu, W. Geological and Geochemical Constraints on the Origin of the Sr Mineralization in Huayingshan Ore District, Chongqing, South China. *Minerals* **2023**, *13*, 279. https://doi.org/10.3390/min13020279

Academic Editor: Jaroslav Dostal

Received: 24 November 2022
Revised: 2 February 2023
Accepted: 13 February 2023
Published: 16 February 2023

Copyright: © 2023 by the authors. Licensee MDPI, Basel, Switzerland. This article is an open access article distributed under the terms and conditions of the Creative Commons Attribution (CC BY) license (https://creativecommons.org/licenses/by/4.0/).

1. Introduction

The average concentration of Sr in the Earth's crust is 0.04%, making it the 15th most abundant element in the crust [1]. Celestine ($SrSO_4$) and strontianite ($SrCO_3$) are the only two valuable minerals rich in Sr [2–4]. However, celestine deposits are the main exploitable Sr deposits in the world [5,6]. Celestine ore bodies usually occur in marine carbonates and evaporites from the Silurian to the Pliocene in layers [7–10]. Based on the geological and geochemical characteristics of the celestine deposits, two principal metallogenic

mechanisms have been proposed: (1) celestine formed by syngenetic precipitation during the evaporation of seawater, and (2) the epigenetic replacement of marine carbonates and sulfates by celestine [10–12].

Huayingshan is located in the southeast of the Sichuan Basin. There are many super-large to large-scale celestine deposits in the Huayingshan, making it the largest strontium resource base in China [13–17]. These celestine deposits share similar geological characteristics, and the orebodies are mainly hosted by marine sedimentary rocks of the Triassic Jialingjiang Formation (T_1j) in layers. Many geological characteristics of these deposits are similar to those of many large celestine deposits in the world (Table 1).

Table 1. Properties of some celestine deposits in the world.

Deposit/Mining Area	Location	Coastal Carbonates and Evaporites	Age of Host Rock	Hydrothermal Activity	Fluid Properties	Celestine $^{87}Sr/^{86}Sr$	Coeval Seawater $^{87}Sr/^{86}Sr$	Interpreted Sr Source	Reference
Montevive	Spain	yes	Miocene	yes	basinal brines and meteoric water	0.7089–0.7086		basinal brines	[18]
Igualada	Spain	yes	Eocene	yes	basinal brines and meteoric water	0.7078	0.7078	evaporites	[19]
Paila	Mexico	yes	Cretaceous	minor	groundwater	0.7077	0.7072	limestones	[20]
Karstryggen	Greenland	yes	Permian	minor	basinal brines	0.7134	0.7068	redbeds	[21]
Ain Allega	Tunisia	yes	Triassic	yes	basinal brined and magmatic-meteoric fluid			carbonates	[22]
Jebel Doghra	Tunisia	yes	Triassic	yes	basinal brines			feldspar-rich series	[5]
Neuquen	Argentina	yes	Cretaceous	yes		0.7072	0.7072	seawater	[23]
Yate	Great Britain	yes	Triassic	no		0.7105	0.7076	limestones	[24]
Ohio basin	United States	yes	Silurian	some	basinal brines			evaporites	[25]
Sivas basin	Turkey	yes	Miocene	yes	magmatic–hydrothermal fluids and meteoric water	0.7078	0.7083–0.7087	evaporites	[26]
Abolfares	Iran	yes	Oligo-Miocene	yes	diagenetic brines			carbonates	[3]
Likak	Iran	yes	Miocene	yes	basinal brines	0.7087–0.7088	0.7083–0.7090	evaporites	[2]
Cyprus	Cyprus	yes	Miocene	yes	basinal brines	0.7089		carbonates	[27]
Huyingshan	China	yes	Triassic	yes	basinal brines	0.7076–0.7078	0.7073–0.7080	carbonates and evaporites	this study
Dafengshan	China	no	Pliocene	no				granite	[28]

Numerous articles on the geological, geochemical characteristics and genesis of the celestine deposit in the Huayingshan have been published [13,15,29–40], but the viewpoints on the genesis of the deposits are inconsistent and can be summarized as follows: (1) Sedimentary deposits related to seawater evaporation [31,40], (2) hydrothermal deposits related to hot brines [13,15,41,42], (3) both sedimentary and hot brine types exist [35].

In this study, we conducted field geological investigation and sampling of the celestite deposits in Huayingshan, and systematically studied the ore-forming fluid characteristics and geochemistry characteristics, including the fluid inclusion of petrography, microthermometry, laser Raman spectroscopy, in situ analysis, and stable isotope measurements (Sr, S) of celestine and country rocks. These new data allow us to better limit the genesis of Sr mineralization in the Huayingshan ore district.

2. Regional Geology

The Huayingshan Sr metallogenic belt is located in the Huayingshan anticlinorium in the SE of the Sichuan foreland basin (Figure 1a). Detailed studies of the geological settings of the Sichuan Basin have been published previously [43–49]. In the study area, tectonic evolution can be divided into two stages: (1) Indosinian, affected by tectonic movements, the study area transformed marine facies to continental facies, and (2) the Yanshanian–Himalayan, affected by tectonic movements, the study area is characterized by intensive lateral compression, forming the Sichuan foreland basin [50–53].

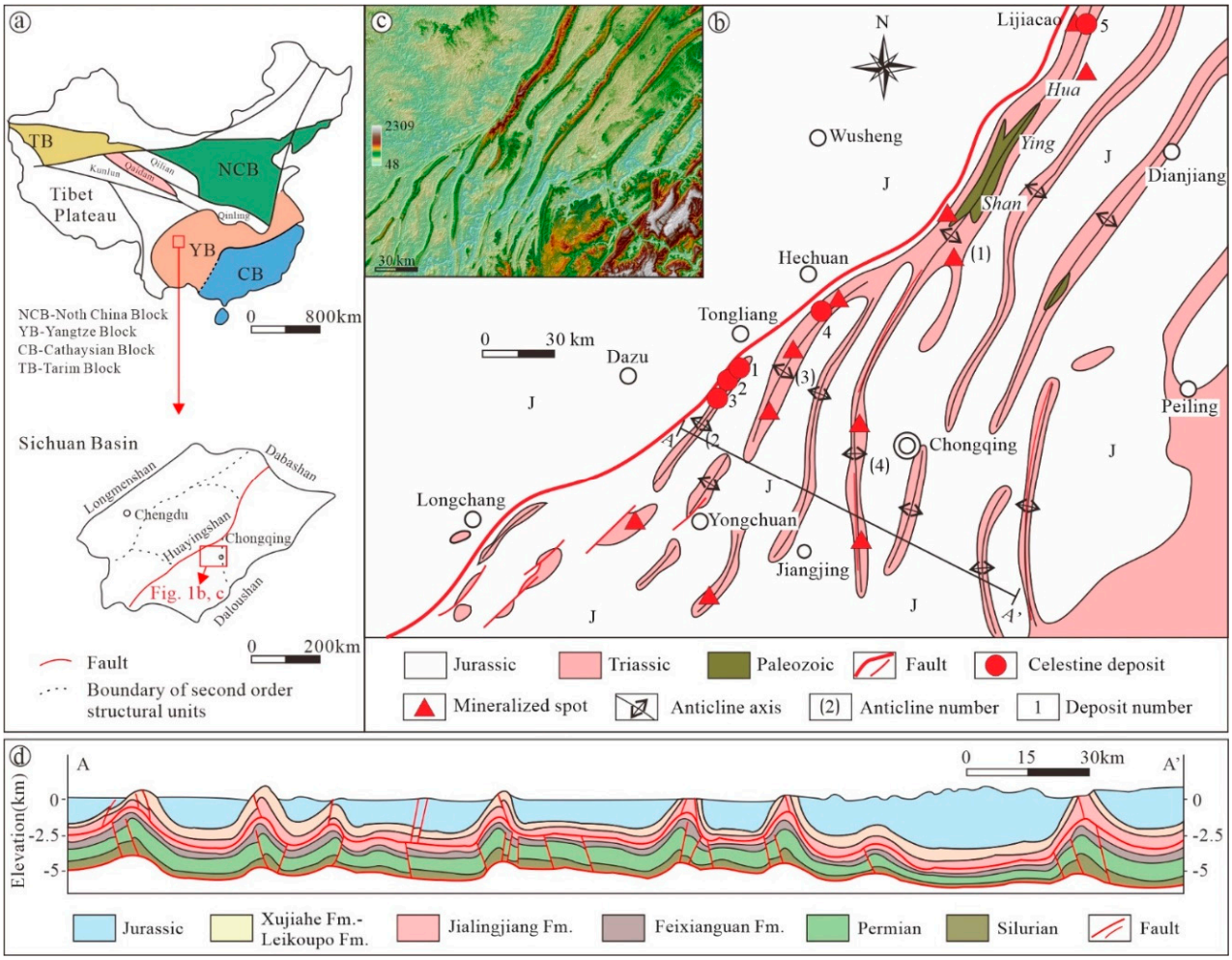

Figure 1. (**a**) Simplified tectonic map of part of China and the Sichuan basin (modified from [46,54]), showing the location of the study area. (**b**) Regional geological map of the Chongqing Sr metallogenic province, showing the distribution of the Sr deposits and mineralized spot (modified from [13]); 1—Yuxia, 2—Chenjiapo, 3—Xinglong, 4—Gangou, 5—Yangtianwo, (1)—Huayingshan, (2)—Xishan, (3)—Libixia, (4)—Guanyinxia. (**c**) DEM of the fold belt in the east of the Sichuan Basin, showing the geomorphic features of the fold belt. (**d**) Geological section through the fold belt in the east of the Sichuan Basin, showing the fault distribution (modified from [55]).

The regional stratigraphic succession comprises the Paleozoic, Triassic, Jurassic, and Quaternary (Figure 1b). The first of these is less exposed in the study area, which is dominated by shale. The second is widely distributed and includes the Feixianugan Formation (T_1f), Jialiangjiang Formation (T_1j), Leikoupo Formation (T_2l), and Xujiahe Formation (T_3xj). The Feixianguan Fm and Xujiahe Fm are dominated by clastic rock, of which the Xujiahe Fm is the main coal-bearing stratum [56,57]. The other two formations are dominated by dolomite and limestone, of which the Jialingjiang Formation is the main reservoir for celestite deposits, natural gas, and geothermal energy [13,58–61]. The Jurassic strata are widely distributed in the study area and are dominated by clastic rocks. Quaternary strata are mainly distributed in low-lying areas, mostly as loose sediments. No magmatic rocks are found in the study area.

The Huayingshan fault is the main fault in this area, with a total length of approximately 500 km (Figure 1b). It plays an important role in controlling the tectonic evolution on both of its sides [53,62,63]. In addition, there are some faults along the fold axis and some buried faults discovered by geophysical methods (Figure 1d) [64]. Affected by Yanshanian–Himalayan tectonic movement, the strata on the southeastern side of the Huayingshan fault

folded and formed many tight anticlines and open synclines, including Xishan anticline, Libixia anticline, Tongluoxia anticline, and Guanyinxia anticline [60]. The anticlines and synclines are alternately distributed, forming a broom-like fold belt [65]. Within this area, the anticlines formed mountains and the synclines formed valleys, forming the geomorphological characteristics of one mountain with two valleys and three ridges (Figure 1c). Celestine deposits are distributed on the southeast side of the Huayingshan fault, mainly in the Xishan anticline (Figure 1b). In addition to celestine deposits, it is also rich in coal, oil, potash, hot spring, natural gas, etc. [13,56,60,61].

3. Deposit Geology

The celestine deposits in the Huayingshan Sr metallogenic belt are mainly distributed in the northern part of the Xishan anticline (Figure 1b), and these deposits have similar metallogenic backgrounds and geological characteristics.

The exposed strata are Triassic and Quaternary (Figure 2). The Quaternary comprises some loose sediments, distributed in low-lying areas. The Triassic includes the Jialingjiang Formation (T_1j), Leikoupo formation (T_2l), and Xujiahe formation(T_3xj) (Figure 3). The T_1j is typically exposed at the axis of the anticline, where the thickness is greater than 500 m thick [66]. It can be divided into four sections (Figure 4): the first member of Jialingjiang Fm (T_1j^1) is dominated by limestone, the upper part of the second member (T_1j^2) is gypsum–salt karst breccia and the lower part is dolomite with interbedded limestone. The third member of Jialingjiang Fm (T_1j^3) is dominated by limestone and the bottom is claystone, and the fourth (T_1j^4) is similar to the second. Regionally, the second (T_1j^2) and fourth (T_1j^4) members of Jialingjiang Fm are characterized by higher Sr content and higher porosity and are the main reservoir of celestine deposits. The T_2l and T_3xj are exposed on both flanks of the anticline. The T_2l is dominated by dolomite, which can be up to 260 m thick, whereas the T_3xj is dominated by clastic rock.

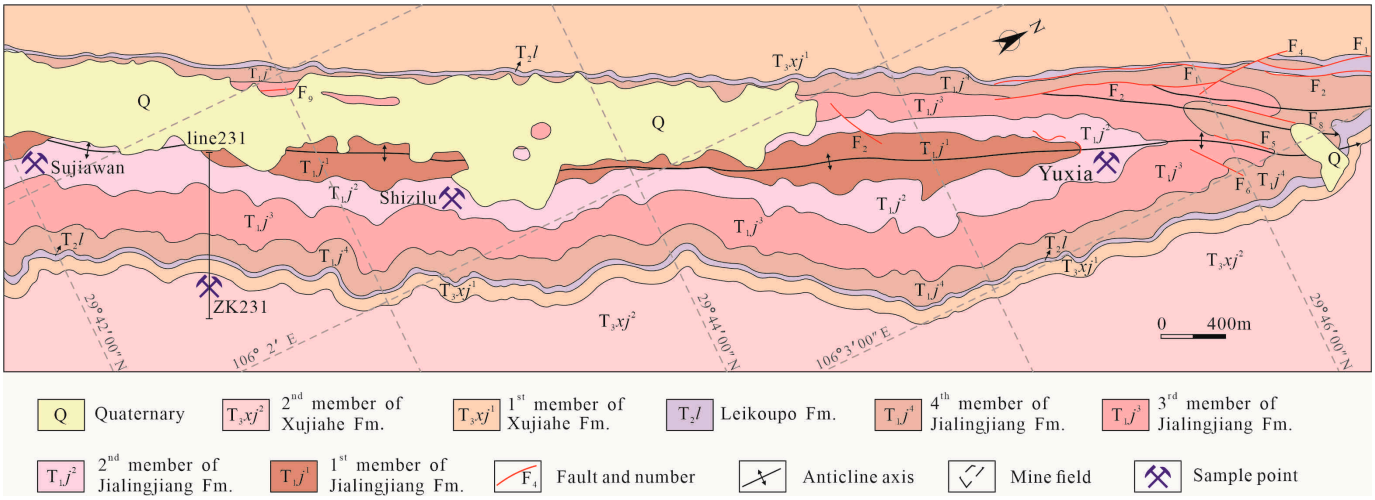

Figure 2. Geological map of the deposits in the Xishan anticline, showing the sampling location.

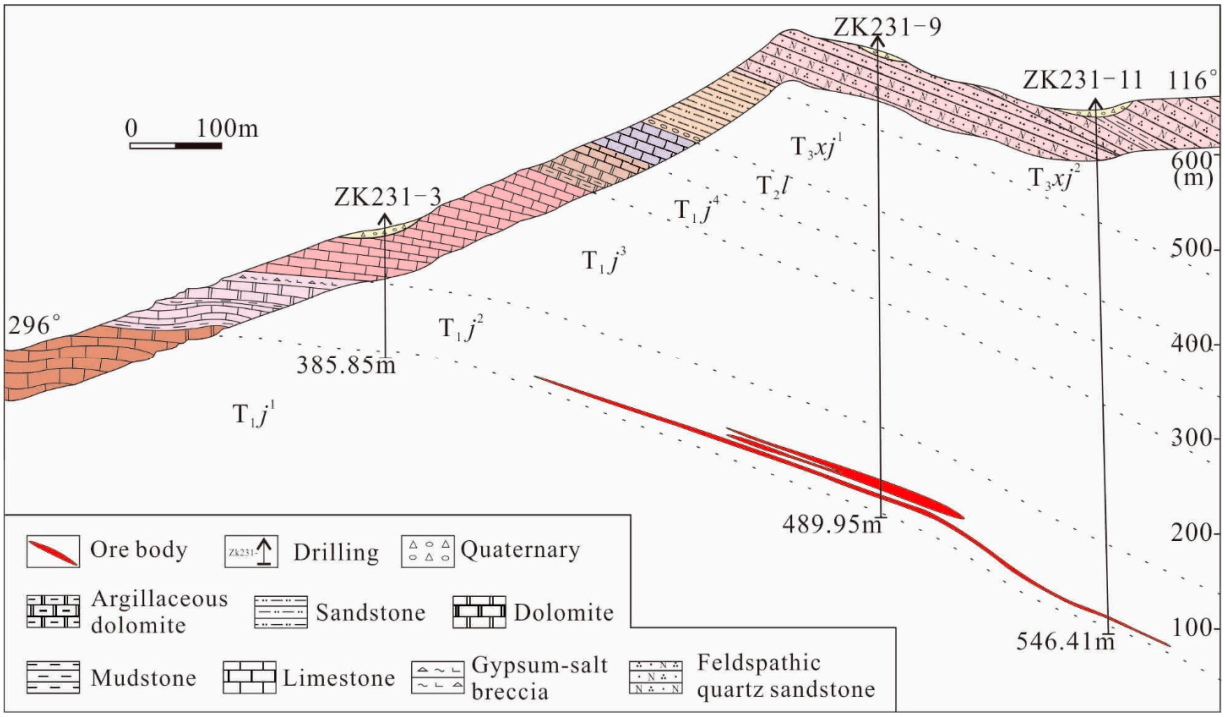

Figure 3. Geological section of the southeast lamb of the Xishan anticline. The location of the section is shown in Figure 2.

Formation	Symbol	Thickness (m)	Profile	Lithology description	Depositional environment
Leikoupo	T_2l^1	35		Dolomitic limestone and limestone	Intertidal and restricted platform
		44		Gypsum - Salt breccia, with green -bean rocks and shale at the bottom and top respectively	
Jialingjiang	T_1j^4	31		Gypsum - Salt breccia	Tidal-flat and restricted platform
		8		Algal dolomite and fine grain limestone	
		15			
		13		Gypsum - Salt breccia	
		7		Limestone and dolomite interbedding	
		22			
	T_1j^3	130		Fine - medium grain limestone	Subtidal and open platform
	T_1j^2	32		Gypsum - Salt breccia	Supratidal and restricted platform
		22		Dolomite and limestone interbedding, dolomite at the bottom contains gypsum	
		40			
	T_1j^1	157		Fine - medium grain limestone	Intertidal and open platform
Feixianguan	T_1f^4	57		Calcareous mudstone with argillaceous limestone	Intertidal and open platform

Figure 4. Synthetic stratigraphy for the fold belt in the east of the Sichuan basin (red symbols represent ore bodies).

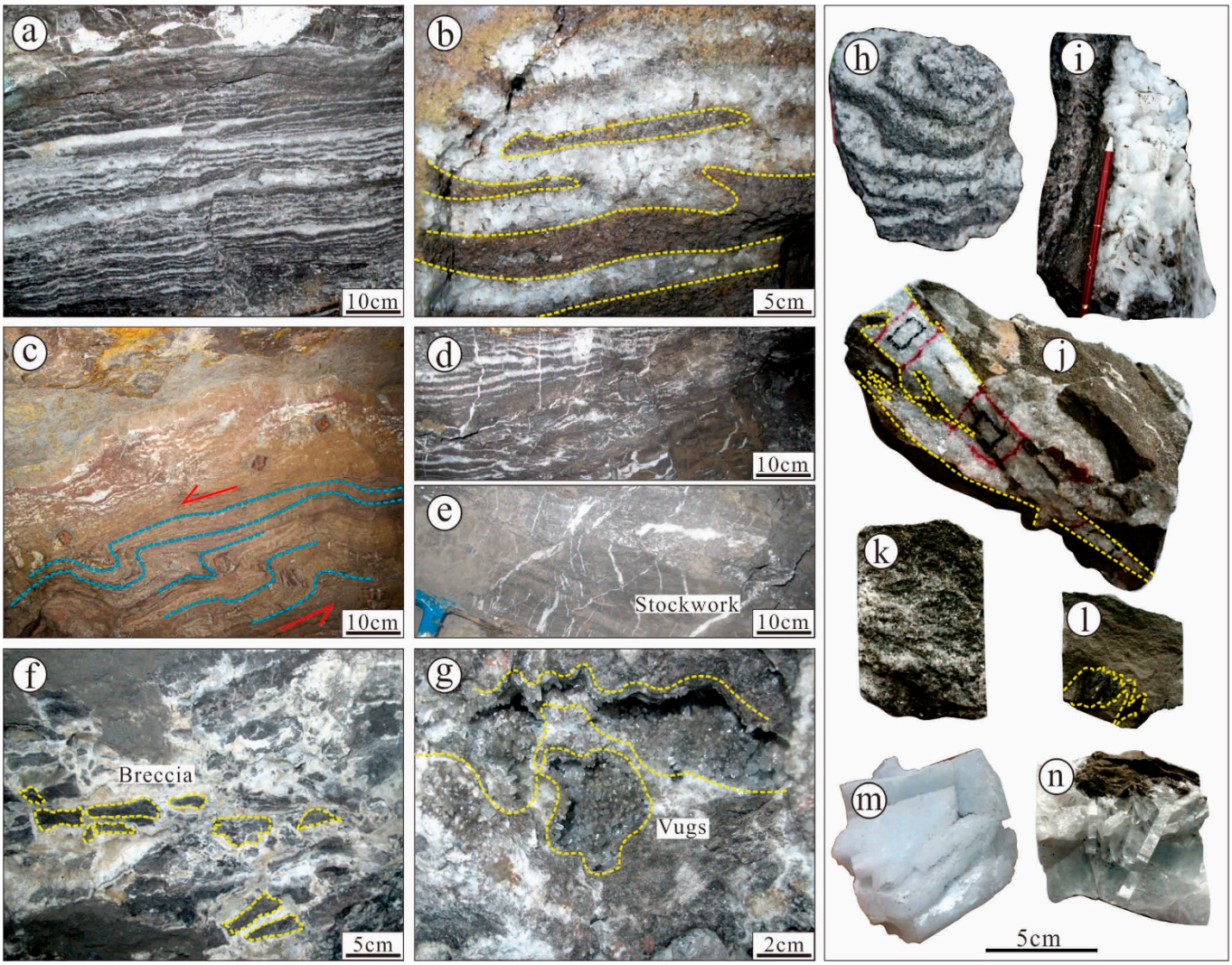

Figure 5. Photographs showing the characteristics of the ore bodies in the underground mine taken at a depth of 305 m and hand specimens collected from underground and drilling. (**a**) Banded celestine in the Jialingjiang Formation. (**b**) Partially enlarged photograph of banded ore, showing that the ore is composed of a dark microcrystalline carbonate band and a white tabular crystalline celestine band. (**c**) Flexure structure in country rock, with red arrows indicating the direction of strata movement. The ore body is not significantly deformed, indicating that it was formed after the tectonic movement. (**d**) Photograph of vein ore and banded ore, showing that they were formed during the same period of hydrothermal activity. (**e**) Reticulate ore. (**f**) Breccia ore; breccia is carbonate, and cement is celestine. (**g**) Photograph of celestine geode, showing celestincrystals as light blue columnar. (**h**) Banded ore. (**i**) White and light-blue celestine clusters. (**j**) Vein ore. (**k**) Disseminated ore. (**l**) Organic vein in dolomite. (**m**) Massive ore. (**n**) Plate-column celestine aggregate.

The ore bodies mainly host in the T_1j^2 and T_1j^4 (Figure 3). Affected by faults and groundwater, the orebody is divided into multiple sections [14], most of which are stratiform (Figure 5a) and stratoid, with some lenticular, veined (Figure 5d), and reticulated (Figure 5e) sections. The structure of ores is common in banded (Figure 4h), massive (Figure 5m), and veined (Figure 5j), followed by brecciated (Figure 5f) and disseminated (Figures 5k and 6d) ores. Some celestine is filled in the vugs (Figure 5g). Ore minerals are mainly composed of celestine, followed by strontianite and barium celestine (Figure 6a). Gangue minerals mainly comprise calcite, dolomite, barite, and gypsum (Figure 6b,c). Celestine is well crystallized, mainly plate-like, granular, and lath-like in shape (Figure 5m,i). The color of celestine crystals is changeable, including colorless, milky white, sometimes

sky blue or light yellow, and it could be light grey. Nevertheless, colorless and milky white crystals are more common. The alteration types mainly include strontianitzation (Figure 6g,h,i) and carbonatization (Figure 6j).

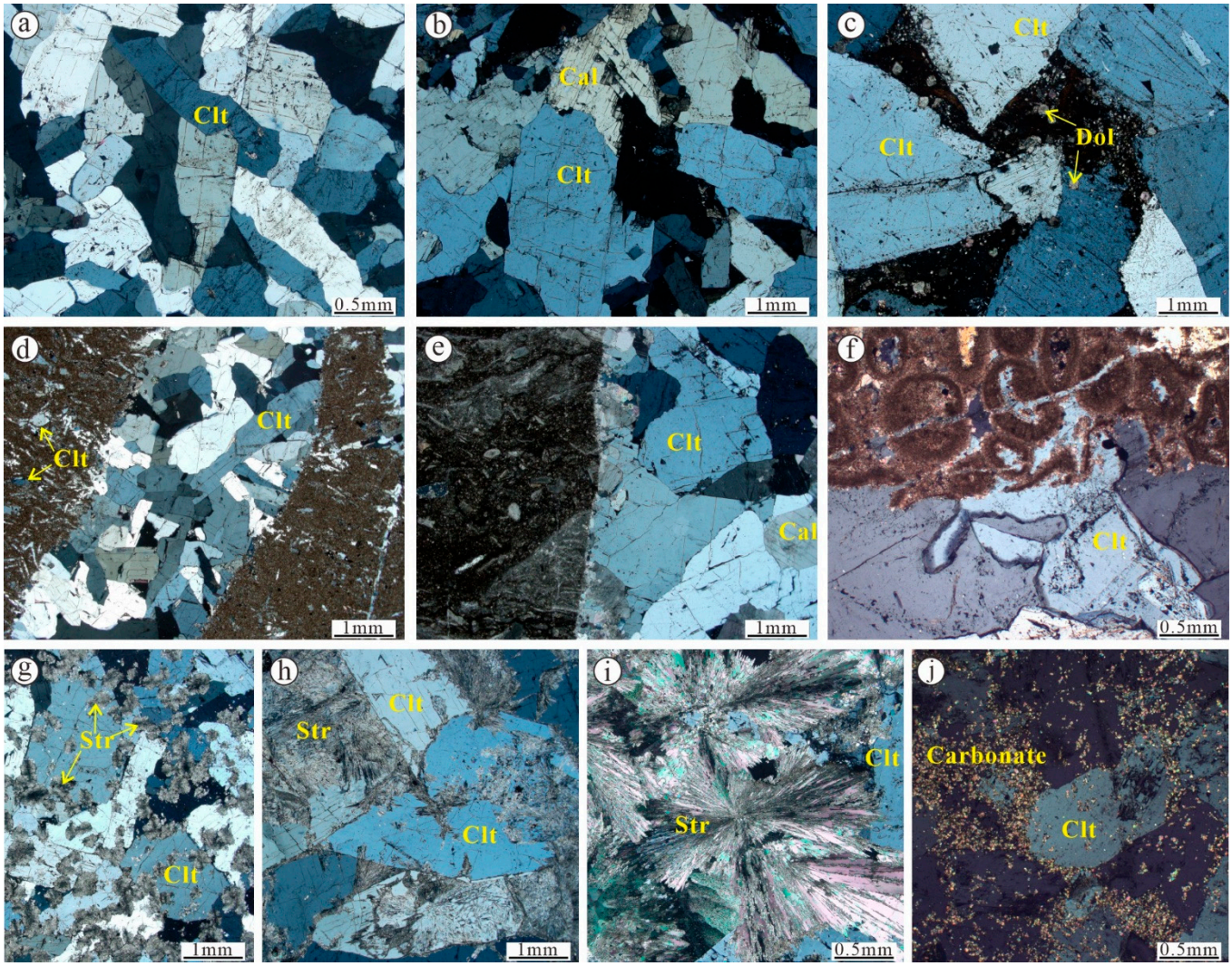

Figure 6. Photomicrographs of ore and gangue minerals in the Yuxia and Xinglong celestine deposits. (**a**) Euhedral–hypidiomorphic tabular celestine. (**b**) Celestine coexists with calcite. (**c**) Dolomite and muddy dolomite exist in the gap of the celestine. (**d**) Veined and disseminated celestine. (**e**) Veined celestine; the wall rock is bioclastic limestone. (**f**). Oolitic limestone was filled and replaced by later celestine. (**g–i**) Different degrees of strontianitzation. (**j**) Carbonatization. Clt = celestine; Cal = calcite; Dol = dolomite; Str = strontianite.

4. Sampling and Analytical Methods

4.1. Sampling

The locations of the samples are shown in Figure 2. Samples named YX- and YX305 were collected from the Yuxia deposit, and those named ZK231-, SJW-, and SZL- were collected from the Xinglong deposit. These samples contain the main types of deposits (Figure 5). In addition to the ore, we also collected the host rocks.

4.2. Fluid Inclusion Study

Twenty-four samples from the main types of ores were used in the fluid inclusion study. The morphological characteristics of fluid inclusions on double-polished thick sections were observed, with a polarized light microscope.

Microthermometry was performed at the Institute of Mineral Resources, Chinese Academy of Geological Sciences, using a Linkam MDS-600 heating–freezing stage attached to a Zeiss microscope. The temperature calibration of the heating–freezing stage was carried out by analyzing standard samples of synthetic fluid inclusions supplied by Fluid Inc. (Oakland, CA, USA). The accuracy of the measurements of the freezing–heating stage from 196 to 25 °C is ±0.1 °C, from 25 to 400 °C is ±1 °C, and from 400 to 600 is ±2 °C. The rate of freezing–heating generally ranged from 1 to 5 °C/min, but when the temperature was close to the homogenization temperature and freezing point of aqueous inclusions, the rate was reduced to 0.2 °C/min. The salinities of fluid inclusions were approximately calculated using the formula for the NaCl–H_2 O system [68].

Laser Raman spectroscopic analyses of fluid inclusions were performed on a LABHR–VIS Jobin Yvon LabRam HR800 Raman microspectrometer at the Analytical Department of Beijing Institute of Geology, China Nuclear Industry Group, using a 532 nm Torus laser as the excitation source and a power of 44 mW. The recording time of the spectrum is 30 s, the size of the spot is 1 μm, ranging from 10 to 4000 cm^{-1}, and the spectral resolution was 1 to 2 cm^{-1}.

4.3. Strontium and Sulfur Isotope

Five celestine samples and seven host rock samples were used for the study of strontium isotopes. Selecting celestine single mineral samples required the use of physical binoculars; the separated samples were washed with diluted HCl and diluted water and dried in an oven, then ground with an agate mortar to 200 mesh, while the rock was directly selected from fresh samples and broken to 200 mesh.

The determination of strontium isotope was completed at the Analytical Department of Beijing Institute of Geology, China Nuclear Industry Group. The strontium isotope determination process is mainly divided into two steps: first, preparation of test solution, and second, determination of strontium isotope ratio. The whole process is completed in the isotope chemistry ultra-clean laboratory and the main instruments used in the experiment are cation exchange column (φ 0.5 cm × 15 cm, AG50 W × 8 (H^+) 100–200 mesh) and a high-precision solid thermal ionization mass spectrometer (IsoProbe-T). NBS987 was used as a standard reference and the precision for strontium isotope measurement is ±0.00003. The detailed test procedure is described in Ref. [69].

Sulfur isotopic analyses of celestine from the study area were carried out at the Institute of Mineral Resources, Chinese Academy of Geological Sciences. The analyses were carried out using 200 mesh pure separates of celestine, which was combusted with Cu_2 O in an oven at 1000 °C and under vacuum conditions. Liberated SO_2 gas was frozen in a liquid nitrogen trap. After cryogenic separation from other gases, the sulfur isotopic compositions were measured with the Canyon Diablo Troilite (CDT) standard on a Thermo–Scientific MAT-253 mass spectrometer with an analytical precision of ±0.2‰. The routine analytical precision for the standard material was ±0.2‰. The results were then calibrated against the standard with a routine analytical precision of ±0.2‰.

4.4. LA–ICP–MS

LA–ICP–MS analysis was performed at The National Research Center for Geoanalysis, Chinese Academy of Geological Sciences, Beijing, China. These analyses used LA–ICP–MS, employing an ELEMENT 2 ICP–MS instrument coupled to a UP-213 laser with a 213 nm wavelength, energy of 2 mJ, pulse frequency of 10 Hz, and beam diameter of 40 μm. NIST610 and KL2-G glass standards were used for internal and external standardization. Each LA–ICP–MS analysis incorporated a ~15 s background acquisition (gas blank) and a 40 s data acquisition from the sample. Every nine-spot analysis was followed by one NIST SRM 610 analysis to correct the time-dependent drift of sensitivity and mass discrimination of the ICP-MS. Reference glasses (NIST610, KL2-G) were analyzed before and after taking the sample measurements. The NIST SRM 610 was used as the external standard, and data reduction was performed using the ICPMSDataCal software (Version 9.0) [70].

5. Analytical Results

5.1. Fluid Inclusion

5.1.1. Fluid Inclusion Petrography

According to the composition of inclusions in the celestine and the proportion of gas phase and liquid phase, four types of fluid inclusions were identified at ambient temperature.

(1). Pure liquid inclusions (PL-type) exist in different types of ores. They are mainly spherical ellipsoids in shape, with a small degree of irregularity, and their long axis diameters are generally from around 2 μm to 10 μm (Figure 7a,b,g). These inclusions are less numerous (approximately 5%) and often occur in association with other types of inclusions.

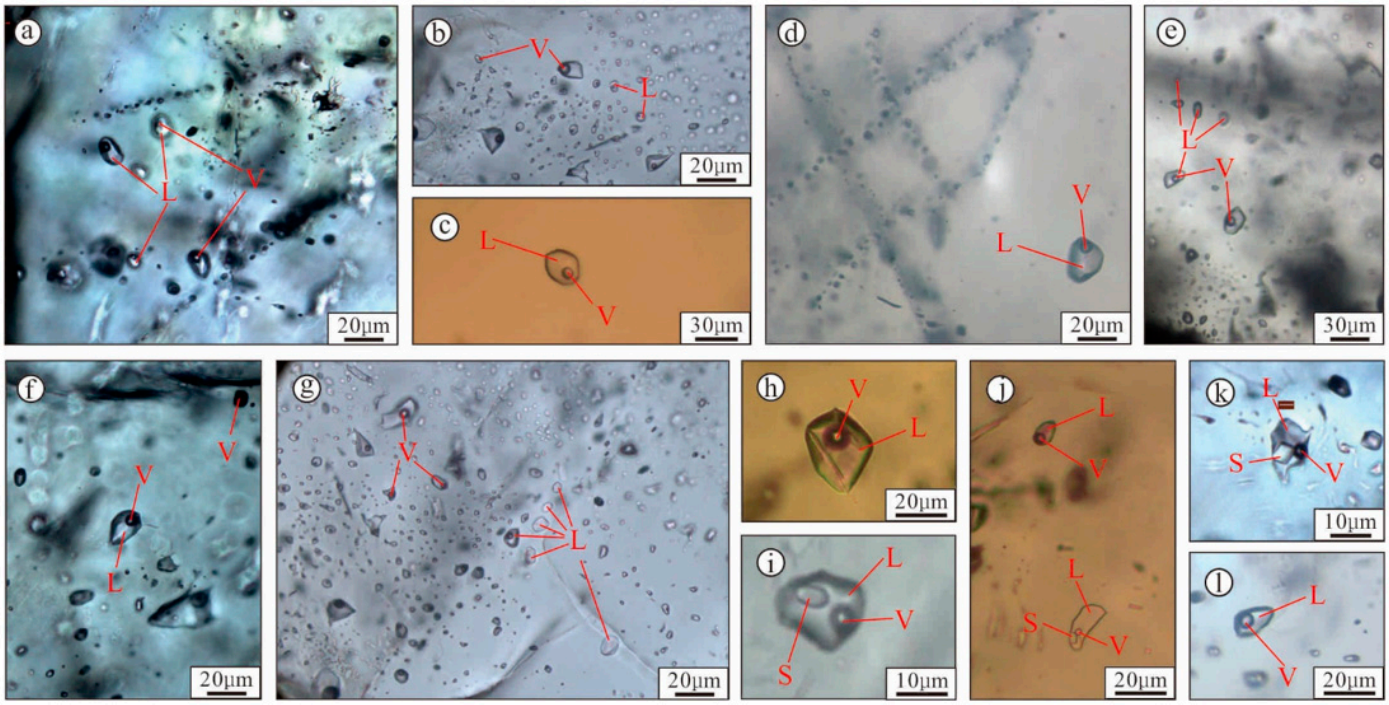

Figure 7. Photomicrographs of fluid inclusions in the celestine deposit in the study area showing representative primary, two-phase (liquid + vapor) fluid inclusions, and three-phase (liquid + vapor + solid) fluid inclusions in the celestine. (**a**) Primary two-phase fluid inclusions and secondary gaseous inclusions, with the latter showing directional orientation. (**b**) Fluid inclusions group. (**c**) Isolated fluid inclusions. (**d**) Isolated primary fluid inclusions and bead-like secondary inclusions. (**e**) and (**f**) are primary two-phase fluid inclusions and pure liquid inclusions. (**g**) Primary two-phase fluid inclusions and pure vapor inclusions. (**h**) Suborbicular fluid inclusion. (**i**) and (**j**) are primary three-phase fluid inclusion, showing that the daughter minerals are rectangular. (**k**) Irregular three-phase fluid inclusion, showing that the daughter mineral is square. (**l**) Oval fluid inclusion.

(2). Pure vapor fluid inclusions (PV-type) are found in various ores. These inclusions are mainly composed of gases and the diameter is generally 3 μm to 5 μm and are mainly spherical and elliptical. They are gray or black under the polarizing microscope (Figure 7f), and there are no phase transitions in the process of heating and cooling.

(3). Two-phase (liquid + vapor) inclusions are the main types of inclusions. They are mainly elliptical and spherical, with partial irregularity, and generally range from 13 μm to 20 μm (few reaching 30 μm) in diameter (Figure 7d). According to the ratios of vapor/liquid, two-phase inclusions can be divided into liquid-rich inclusions (liquid/vapor > 1) (Figure 7a,b,d) and vapor-rich inclusions (liquid/vapor < 1) (Figure 7c). The former is the main type, often appearing in groups with pure vapor fluid inclusions and pure liquid inclusions, which homogenize with the liquid phase after heating.

(4). Three-phase (liquid + vapor + solid) inclusions are rare and can only be seen occasionally. The morphology of three-phase inclusions is various and mainly irregular (Figure 7i,j,k). The shape of daughter minerals in inclusions is rectangular or nearly rectangular, and the length is generally bewteen 3 μm and 6 μm.

Among the four kinds of celestine ore samples, the fluid inclusions in the banded ore and vein ore are abundant and larger, and they are distributed in groups.

5.1.2. Microthermometry

Only two-phase liquid-rich fluid inclusions were used to measure ice-melting and homogenization temperatures, and they were randomly selected from primary inclusions in the good crystal of the celestine. The homogenization temperature and salinity of 796 fluid inclusions are shown in Table 2 (the salinity of some inclusions has not been tested successfully). Fluid inclusions in ZK231- samples have a wide range of homogenization temperatures, ranging from 173 °C to 330 °C, with most numbers clustered from around 200 °C to 220 °C, and ice-melting temperatures ranging from –2.6 °C to –8.8 °C, corresponding to 3.6 wt% to 12.6 wt% NaCl equiv., with most numbers clustered from 7 wt% to 8 wt% and from 10 wt% to 12 wt% NaCl equiv. (Figure 8a,b).

Table 2. Summary of the microthermometric data of fluid inclusions in the celestine from the celestine deposits in the Xishan anticline. (Numbers in parentheses represent the number of measurements, and T_h represents homogenization temperature.)

Sample No.	Type	Characteristics of Inclusions		Salinity (wt% NaCl Equiv.)	T_h (°C)
		Size (μm)	Vapor Volume (%)		
ZK231-444.75	vein	3–24	5–15	5.6–11.7 (26)	190–330 (27)
ZK231-452.45	vein	3–27	5–20	4.3–12.6 (34)	173–345 (37)
ZK231-458.15	vein	2–15	5–20	5.3–11.1 (26)	192–221 (38)
ZK231-460.45	massive	5–17	10–20	10.2–12.0 (35)	211–232 (43)
ZK231-465.05	striped	4–19	5–20	3.6–11.6 (34)	181–229 (40)
YX305 S2	massive	3–21	5–25	0.9–4.8 (48)	157–278 (55)
YX305II3	striped	5–18	5–20	2.1–5.4 (34)	148–276 (44)
YX305 S3③	vein	3–15	5–15	5.9–8.1 (22)	192–242 (26)
YX305 S3②	vein	3–17	5–15	2.6–9.1 (26)	177–258 (26)
YX305 S3①	vein	4–20	5–15	0.7–11.7 (32)	165–277 (34)
YX305II1	striped	3–16	5–15	3.7–8.0 (45)	167–283 (45)
YX305II-2	striped	3–19	5–20	2.9–5.9 (39)	182–224 (45)
YX-H2	striped	7–23	5–15	1.6–9.7 (33)	152–315 (35)
YX-H3	striped	5–20	5–20	2.7–6.7 (46)	172–297 (44)
YX-H5	striped	6–22	10–20	2.6–10.5 (33)	106–300 (31)
YX-H6	striped	3–23	5–15	4.0–11.9 (30)	180–297 (32)
SJW-H9	striped	5–21	5–20	5.1–10.0 (32)	169–263 (33)
SJW-H8	striped	3–25	5–20	1.4–8.3 (32)	173–262 (32)
SJW-H5	striped	3–20	5–20	4.7–13.5 (31)	174–313 (31)
SJW-H4	striped	3–15	5–25	7.9–11.7 (28)	147–221 (28)
SJW-H1	massive	3–10	10–25	5.3–9.0 (10)	199–262 (10)
SZL-H1	massive	4–14	10–20	5.7–13.4 (20)	195–300 (20)
SZL-H2	striped	3–17	5–25	5.7–11.6 (20)	140–271 (20)
SZL-H3	striped	5–15	5–20	6.9–10.9 (20)	166–222 (20)

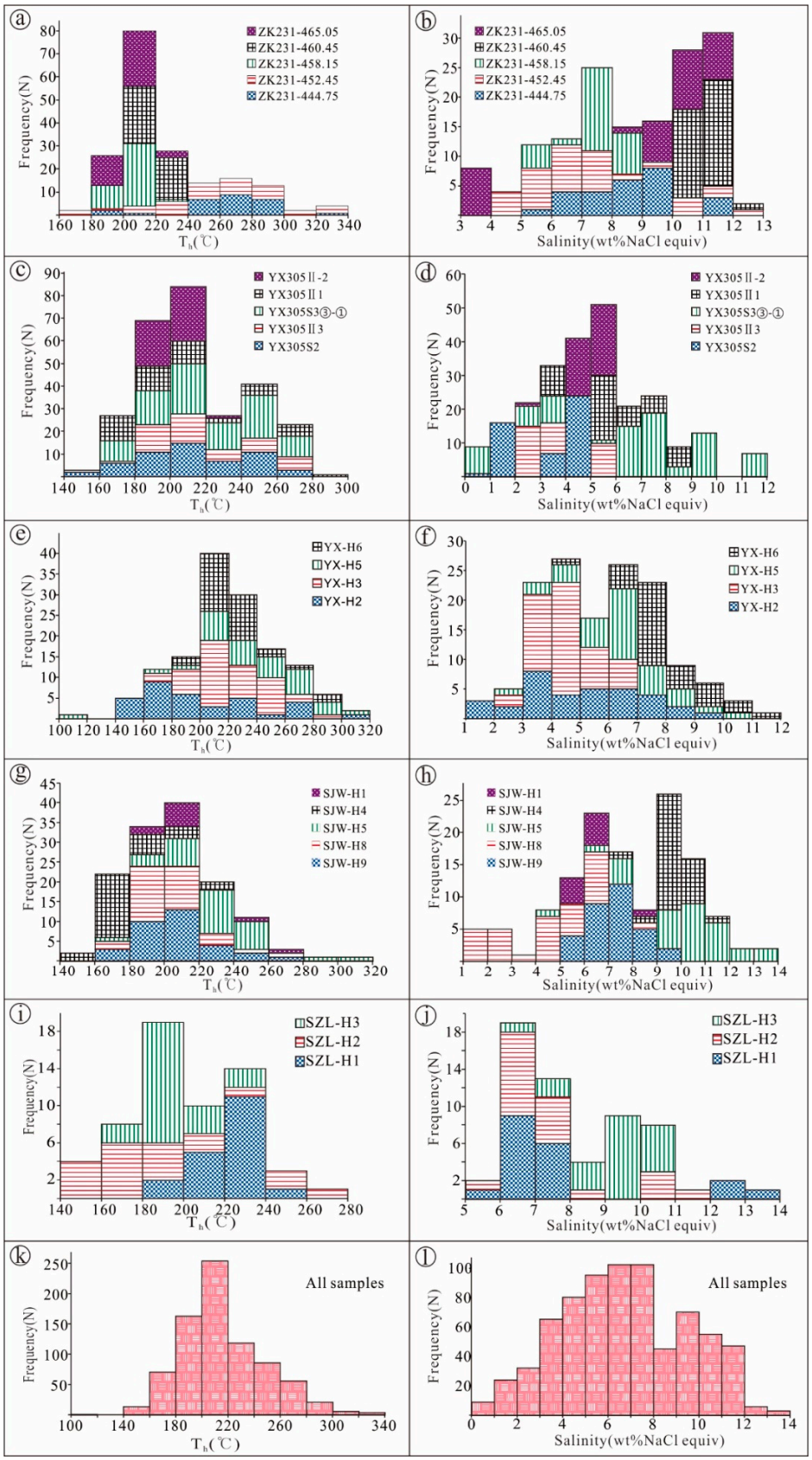

Figure 8. Histograms of homogenization temperatures and salinities of fluid inclusions in celestine in different types of ores (**a**–**j**) and all test results of fluid inclusions (**k**,**l**). See Figure 2 for sample locations and Table 2 for sample types.

The homogenization temperature of fluid inclusions in YX305- samples, at a range of 148 °C to 283 °C with maximum frequency from 200 °C to 220 °C, at an ice-melting temperature between −0.5 °C and −11.3 °C, corresponding to 0.9 wt% to 11.7 wt% NaCl equiv.

With most numbers clustered around 5 wt% to 6 wt% NaCl equiv. (Figure 8c,d). The microthermometry results of fluid inclusions in YX- samples are similar to those of fluid inclusions in YX305- samples (Figure 8e,f).

The homogenization temperatures of fluid inclusions in SJW- samples range from 147 °C to 313 °C, and their ice-melting temperatures range from −0.8 °C to −9.6 °C, corresponding to 1.4 wt% to 13.5 wt% NaCl equiv., with most numbers clustered around 6 wt% to 7 wt% NaCl equiv. and 9 wt% to 10 wt% NaCl equiv. (Figure 8g,h).

The homogenization temperatures of the fluid inclusions in the SZL- samples, ranging from 140 °C to 300 °C, mostly clustered around 180 °C to 200 °C and 220 °C to 240 °C, with their ice melting temperatures ranging from −3.5 °C to −9.5 °C, corresponding to 5.7 wt% to 13.4 wt% NaCl equiv. (Figure 8i,j). The distribution of their salinity is not obvious, partly concentrated in the 6 wt% to 8 wt% NaCl equiv., whereas the other part is distributed between 9 wt% and 11 wt% NaCl equiv. A possible reason for this phenomenon is that some of the inclusions are affected by cracks or cleavage.

The statistics of all the test results show that the homogeneous temperature of fluid inclusions is concentrated between 200 °C and 220 °C (Figure 8k), and the salinity of fluid inclusions is concentrated between 6 wt% and 8 wt% NaCl equiv. (Figure 8l). The ore-forming fluid has the characteristics of medium temperature and high salinity (Figure 9).

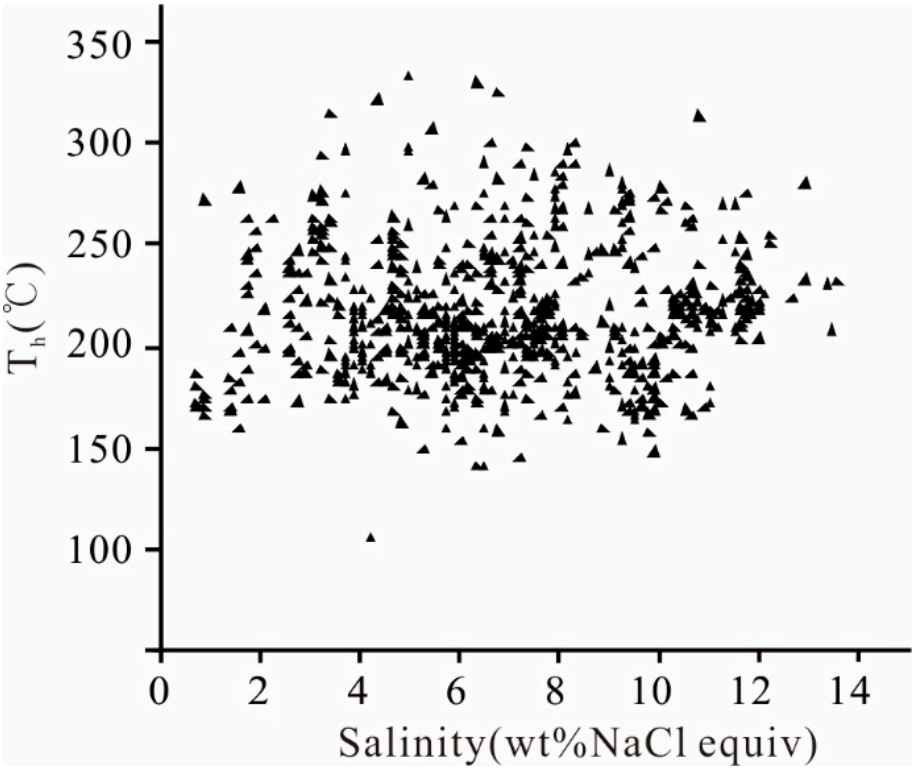

Figure 9. Summary plot of homogenization temperatures and salinities of fluid inclusions.

5.1.3. Laser Raman Spectroscopy

Laser Raman (LR) microspectroscopy analysis was performed on different types of fluid inclusions. The LR results of individual fluid inclusions indicated that H_2O dominated the liquid phase of the fluid inclusions in different types of ores, and the vapor phase component is CH_4 (Figure 10). Unfortunately, the composition of neutron crystals in the fluid inclusions was not detected in this study.

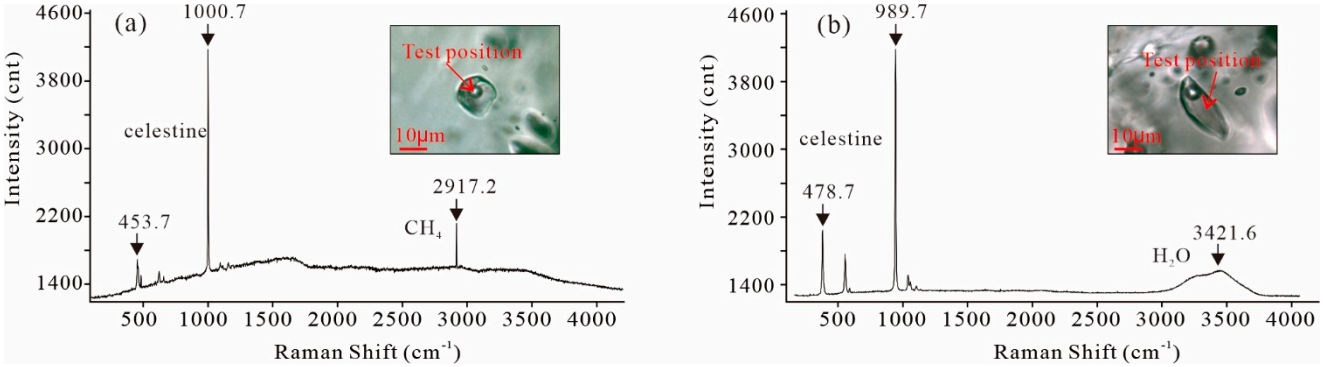

Figure 10. Representative Laser Raman spectra for fluid inclusions from the celestine deposit in the Xishan anticline. (**a**) vapor phase composition of fluid inclusion. (**b**) liquid phase composition of fluid inclusion.

5.2. Sr-S Isotopes

The Sr isotope ratios of celestine and host rocks are listed in Table 3. Five samples of celestine have $^{87}Sr/^{86}Sr$ ratios from 0.7076 to 0.7078, and seven host rocks have $^{87}Sr/^{86}Sr$ ratios from 0.7077 to 0.7080 (Figure 11).

Table 3. Sulfur isotopic and strontium isotope composition of celestine and country rocks from the Huayingshan area.

Deposit	Sample No.	Type	Sr		$\delta^{34}S$ (‰)	Comment
			$^{87}Sr/^{86}Sr$	2σ		
Yuxia	YX305 S3	dolomite	0.7078	0.000011		this study
	YX305 S1	dolomite	0.7077	0.000012		
	YX305II1	dolomite	0.7078	0.000011		
	YX305II2	dolomite	0.7077	0.00001		
	TL-3	massive celestine	0.7078	0.000011	36.9	
	TL-5	massive celestine	0.7077	0.000014	36.8	
	TE-1	celestine	0.7087			[34]
	TE-2	celestine	0.7089			
	TT-4	dolomite	0.7088			
	TT-9	dolomite	0.7089			
Xinglong	ZK231-444.75	dolomite	0.7080	0.000017		this study
	ZK231-455.75	dolomite	0.7077	0.000016		
	ZK231-471.25	dolomite	0.7077	0.000011		
	YX305 S1	banded celestine	0.7078	0.000013	39.0	
	YX305II3	banded celestine	0.7076	0.000011	36.8	
	ZK231-455.75	celestine vein	0.7078	0.000009	36.4	
	ZK231-452.45	celestine			36.9	
Hechuan	HC-S27	banded celestine	0.7078			[71]
	HC-S2	banded celestine	0.7085		34.5	
	HC-S18	massive celestine	0.7078		37.6	
	HC-S24	brecciated celestine	0.7094		32.5	
	HC-S22	massive celestine	0.7072			
	HC-1	reticulate celestine	0.7068		35.3	
Gongqiaoba	A2-1	celestine	0.7105		35.92	[34]
	A3-1	celestine	0.7098		36.12	

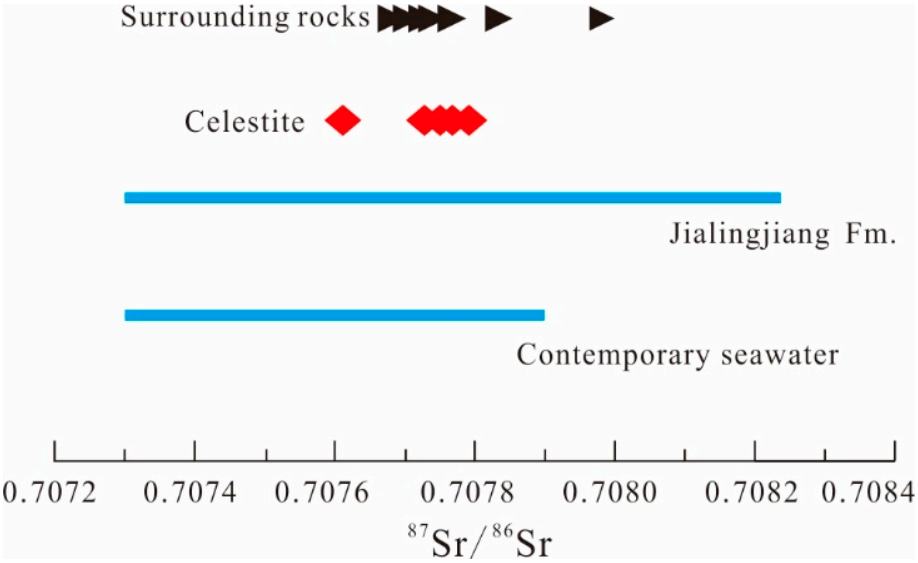

Figure 11. Sr isotopic compositions of celestine and host rocks. Sr isotope data of the Jialingjiang Formation and contemporaneous seawater are obtained from [72,73].

Six samples of celestine were selected for the sulfur isotope test, and the data are listed in Table 3. Except for the $\delta^{34}S$ value of YX305 S1, which is 39.0 ‰, the $\delta^{34}S$ values of other samples are in a narrow range, ranging from 36.4 ‰ to 36.9 ‰ (Figure 12).

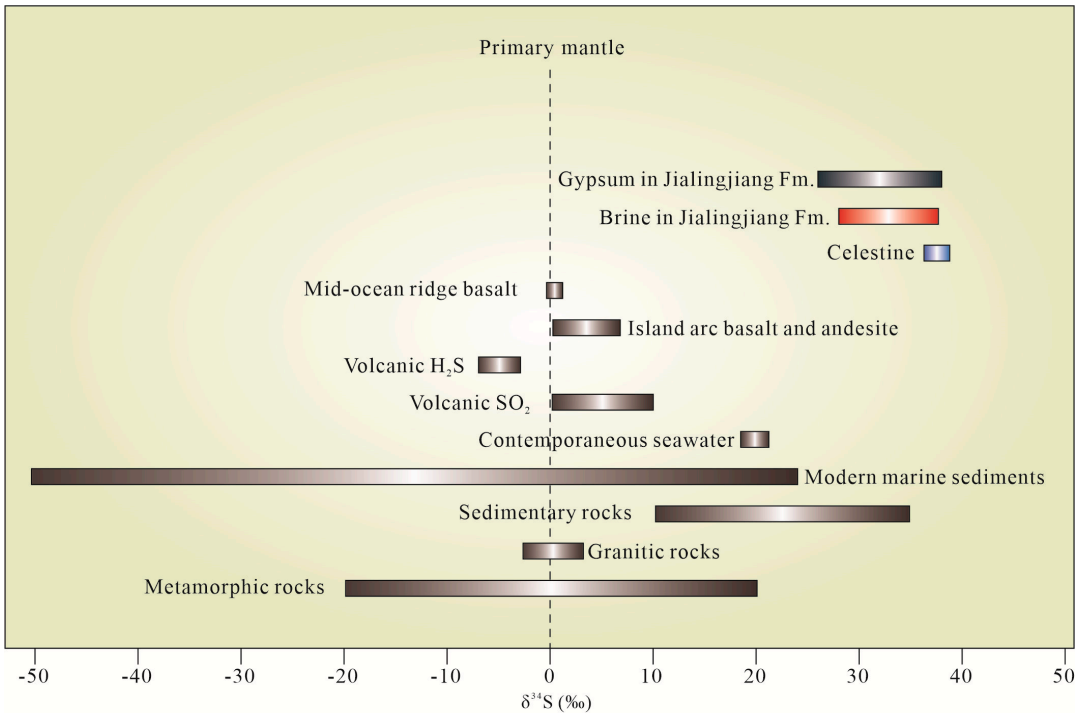

Figure 12. S isotopic compositions of celestine. S isotope data of the gypsum and brine in the Jialingjiang Formation are obtained from [74].

5.3. Major and Trace Elements

Many elements (including major elements and trace elements) are below the detection limit, especially rare earth elements, which are similar to other celestine deposits around the world. In this study, only the test results of CaO and Sr were selected. The results are

shown in Table 4. There was a negative correlation between CaO and Sr content (R^2 = 0.95) (Figure 13).

Table 4. Sr and CaO content of in situ analysis of celestine.

Spot	CaO (wt. %)	Sr (ppm)
yx305 s-2_1	32.4	226,725
yx305 s-2_2	40.7	145,667
yx305 s-2_3	32.3	227,958
zk231-465-1	30.9	249,758
zk231-465-2	43.6	107,998
zk231-465-3	30.1	249,852
zk231-465-4	29.0	265,361
zk231-465-5	29.6	262,730
zk231-465-6	30.0	254,193
zk231-465-7	31.3	242,441
zk231-465-8	29.4	258,119
zk231-458-1	30.9	250,319
zk231-458-2	30.2	257,271
zk231-458-3	30.6	253,011
zk231-458-4	30.2	256,737
zk231-468-2	25.1	284,900
zk231-468-3	31.3	247,194
zk231-468-4	29.3	261,366
yx305 II1-1	30.4	251,458
yx305 II1-2	29.5	263,088
yx305 II3-1	28.8	270,634
yx305 II3-2	27.4	255,012
yx305 II3-3	28.7	249,488

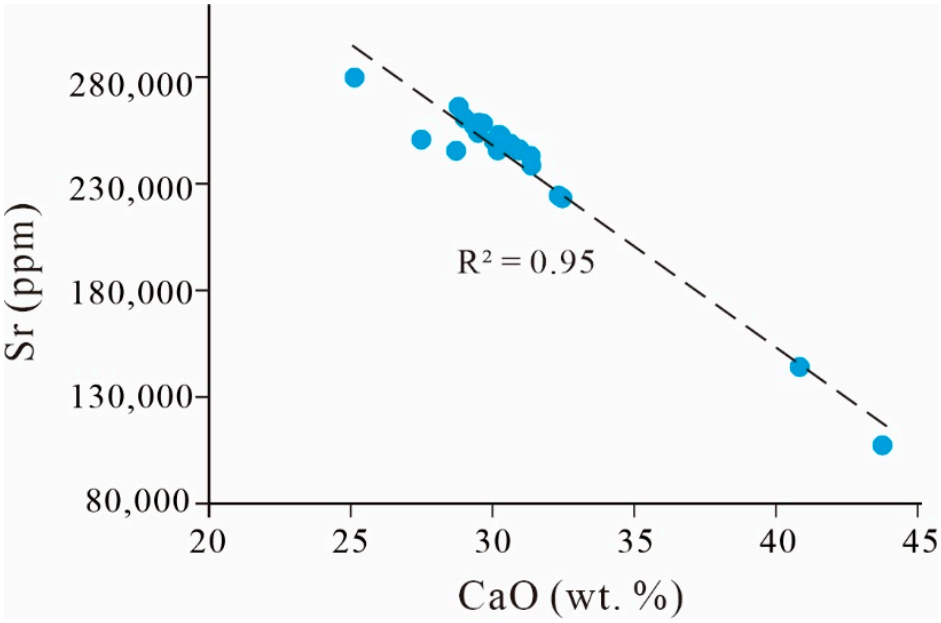

Figure 13. Correlation coefficients of Sr and Cao in samples from the celestine deposits in Xishan anticline.

6. Discussion

6.1. Nature of the Mineralizing Fluid

In this study, the fluid inclusions in celestine were homogenized at temperatures ranging from 100 °C to 340 °C, mostly between 200 °C and 220 °C, indicating that the mineralization of celestine is related to hydrothermal activity, and other evidence for coeval hydrothermal activity has been detected in the study area [75,76]. The formation of many

large celestine deposits in the world is related to hydrothermal activities, which are mainly basinal brine [2,3,5,19,20,25,77–79], some of which are related to magmatic–hydrothermal activities [22,80]. The source of basinal brines is complex. Paleoseawater, meteoric water, and diagenetic fluid (pore water and crystal water) are all important sources of basinal brines [81,82]. The ore-forming fluids of most celestine deposits related to the hydrothermal activity are characterized by meso-low temperature and high salinity [5,10,79,80].

No obvious evidence of magmatic activity has been detected in Huayingshan since the Permian, and most of the previous research suggests that the mineralization of celestine deposits in Huayingshan is closely related to the activity of basinal brines, but not related to the magmatic activity. From the Triassic to the Himalayan [13,17], the Sichuan Basin experienced a complicated geological evolution. Similarly, the brines in the basin also experienced a complex evolutionary process, and their composition should be complex in result [83].

Based on the study of H-O isotopes of celestine in the Huayingshan Sr metallogenic belt, Zhu et al. [34,41] concluded that the basinal brines were formed by the mixture of formation water and meteoric water. Li [29,30] believed that the fluid mainly derived from pore water, crystal water, or structural water discharged during diagenesis and compaction of carbonate and evaporite. Huang et al. [37,84] believed that a large amount of freshwater formed by thermochemical sulfate reduction (TSR) is a significant component of the basinal brines. Zhou determined that the brines originated from Paleoseawater by studying the H-O isotopes of the Triassic formation brines in the east of the Sichuan Basin [85]. The microthermometry results show that the ore-forming fluid is characterized by meso-low temperature and low salinity. Combined with the regional geological background and published H-O isotope results [41], we believe that large meteoric water is the main source of basinal brines, and the rapid supply of a large amount of meteoric water along the faults (mainly Huayingshan fault) is the main factor causing the low salinity of ore-forming fluid. In addition, the TSR process widely exists in the Triassic strata in the east of the Sichuan Basin [86–88], and the water formed in this process also reduces the salinity of the fluid. The results of LR microspectroscopy analysis show that the gas phase composition of inclusions in various types of celestine is mainly CH_4, and there is no similar study on other celestine deposits around the world. We inferred that the CH_4 in the fluid inclusions derives from the paleo-gas reservoir. The eastern Sichuan Basin is rich in gas, which will destroy some gas reservoirs in the process of tectonic movement, resulting in the release of CH_4 dissolved in the fluid. The existence of organic matter in the fractures of the host rock supports this view.

There are several previous studies on the characteristics of ore-forming fluids of celestine deposits in the Huayingshan Sr metallogenic belt [15,29,41], but the results and conclusions are inconsistent. Most suggested that there are three stages of hydrothermal activity during the formation of the deposit: in the first stage, brine activity (220–300 °C) forms banded ore; in the second stage, brine (150–220 °C) fills the host rock fissures to form massive and vein ore; and in the third stage, brine (<150 °C) fills along the faults to form celestine and barite veins [15,16,33,89]. It is also believed that the low homogenization temperature (60–70 °C) of inclusions in banded ore is due to deposition, while the relatively high homogenization temperature (160–170 °C) of inclusions in massive ore is related to hot brine activity [39]. One of the important reasons for the difference in the microthermometry results and conclusions of the fluid inclusions in the celestine is that the temperature measurement data are limited. In this study, 796 tests were carried out on the homogenization temperature of fluid inclusions in different types of celestine from different mining areas. The results show that the homogenization temperature of fluid inclusions in different types of celestine has no obvious difference, and the peak value of homogenization temperature has a good consistency, indicating that different types of ores in the study area may be formed by the same phase of the fluid. Different spaces lead to different types of ores. Because of the lack of magmatic activity, the heat of ore-forming fluid should originate from geothermal heating; however, the maximum burial depth of Triassic strata

is seven kilometers, and the maximum temperature is 200 °C [61], which is smaller than the homogenization temperature of the fluid inclusions in celestine [76], which indicates that ore-forming fluid has experienced a deeper cycle. Through geophysical exploration, it was determined that the Huayingshan fault is a deep fault, along which basic rocks are found. The celestine deposits and modern hot springs are mainly distributed along the Huayingshan fault [60,90], indicating that it is the main channel for fluid migration.

6.2. Sources of Ore-Forming Matter

6.2.1. Source of Strontium

Sr is the main element of the celestine, and Sr isotope analysis is widely used to identify the sources of Sr in the celestine [1,18,23,91]. Most of the celestine deposits located around the world are mainly hosted in marine carbonates and evaporites [92,93], and the Sr isotope value of celestine is consistent with/or slightly different from that of coeval seawater [10], indicating that the formation of celestine deposits is closely related to seawater, and some authors state that the mineralization age of the deposit by comparing the Sr isotope ratio of celestine with that of seawater [2,27].

The Sr isotope ratios of celestine and host rock measured in this study are 0.7076–0.7078 and 0.7077–0.7080, respectively, which shows good consistency, and these values are within the Sr isotope values of the Jialingjiang Formation and contemporaneous seawater [73,94–98], indicating that the formation of celestine deposits is closely related to pale seawater. The formation of celestine deposits in the Huayingshan strontium metallogenic belt is related to brine activity, and the metallogenic age is later than the diagenetic age. The characteristics of many large celestine deposits around the world are similar to those in the Huayingshan [10], and the formation of these deposits has undergone the following two stages: (1) preconcentration of Sr in formation during evaporation; and (2) dissolution of Sr in formation during brines circulation. We believe that the formation of celestine deposits in the Huayingshan area also includes the above two stages. The first stage is related to the lithofacies paleogeography of the Early Triassic in the study area. Influenced by the Indosinian Movement, the Sichuan Basin gradually evolved from an "ocean basin" to a "solitary basin", and the study area in Sabkha during the Early Triassic formed the gypsum salt layer [99,100]. Some researchers suggest that celestine ore bodies can be formed during seawater evaporation [23,40], while some others disagree and believe that during the process of seawater evaporation, Sr is mainly concentrated in aragonite and biological carbonate [101,102], and celestine ore bodies cannot be formed. Some clastic and carbonate rocks formed in Sabkha have high strontium content, which proves that Sr can be enriched during evaporation [103], but determination of whether it can form celestine ore bodies requires further research. The second stage, in which there is more Sr enriched in the brines, is important for the formation of celestine deposits, and many celestine deposits around the world have experienced the process of Sr re-enrichment [2,3,20,24,25]. The methods for enriching Sr into brines include the following: (1) Aragonite-calcite conversion: the Triassic sedimentary environment is favorable for aragonite precipitation. Due to the geochemical behavior of Sr, aragonite generally contains abundant Sr (up to 10,000 ppm) [104]. During the diagenetic process, aragonite turns into calcite, releasing a large amount of Sr^{2+} to pore water [84,105,106], which converge into brines under compaction. (2) Dolomitization: compared with dolomite, limestone is rich in Sr, indicating that a large amount of Sr^{2+} may be released during dolomitization [107], and this Sr^{2+} will eventually enter the brines. Due to the high solubility of the celestine [108], it is impossible to enrich a lot of SO_4^{2-} and Sr^{2+} together in solution, and high salinity fluid is beneficial to increase Sr concentration. The salinity of ore-forming fluids in many celestine deposits is high, but the salinity of ore-forming fluids in the Huayingshan Sr metallogenic belt is low. Therefore, only reducing the concentration of sulfate in the fluid can increase the concentration of Sr in the fluid. TSR and bacterial sulfate reduction (BSR) can consume sulfate in the fluid, resulting in higher Sr concentration in the fluid. Moreover, in Fe-deficient sediments, the activity of bacteria will reduce the pH and promote the dissolution of biogenic carbonate [101,109], releasing Sr^{2+} into the pore water [19].

Some published Sr isotope values are higher than the Sr isotope values obtained in this study and higher than the Sr isotope values of the Jialingjiang Formation. Previous studies have pointed out thatthat the brines have dissolved the strontium of other strata in the process of circulation [30,34]. However, we concluded that the strontium dominantly derives from the Jialingjiang Formation. The reasons are as follows: First, the Jialingjiang Formation has a high strontium content, and the ore-bearing stratum is also the Jialingjiang Formation. Second, as with the aquiclude, the mudstone and shale interlayer with low permeability in the formation can restrict the material exchange between the strata, and the material exchange between the formations mainly passes through the fracture, with low efficiency. Third, most of the Sr isotopic values of the celestine are consistent with those of the Jialingjiang Formation.

6.2.2. Source of Sulfur

The $\delta^{34}S$ values of most samples are in a narrow range, ranging from 36.4‰ to 36.9‰, which is close to Hechuan and Gongqiaoba celestine deposits [30,34], indicating that the celestine deposits in the Huayingshan Sr metallogenic belt have the same sulfur source. In the Early Triassic, the $\delta^{34}S$ values of strata in the east of the Sichuan Basin were significantly higher than those of seawater [110–112], and the $\delta^{34}S$ values of the celestine in the Huayingshan Sr metallogenic belt were higher than those of coeval seawater. However, the range of sulfur isotope values of the Jialingjiang Formation [74,110] indicates that the S may derive from the Jialingjiang formation.

The $\delta^{34}S$ values of many celestine deposits are higher than that of coeval seawater [18,19,27], and other deposits associated with marine carbonates and evaporites, such as Au, Pb, and Zn, also have this characteristic [113–116]. The reason for that is complex; it can be caused by S fractionation or by the mixing of sulfur from different sources. TSR and BSR are two significant processes of S fractionation in celestine deposits [92,117]. BSR usually occurs during diagenesis at 0 to 80 °C [109], while the lowest temperature of TSR is 127 °C [118,119]. During Indosinian period, the study area was an evaporation environment, and BSR may be the main factor leading to the abnormally high $\delta^{34}S$ values of the Jialingjiang Formation. The study shows that BSR can produce from 30‰ to 40‰ high fractionation [109], and the $\delta^{34}S$ values of the Jialingjiang Formation conform to this feature. During the diagenesis, sulfate reduction widely existed in the lower Triassic in the east of the Sichuan Basin [120], and the sulfur fractionation by the TSR process is generally less than 20‰ [121,122]. After the BSR process, the $\delta^{34}S$ values of diagenetic fluid and brines increased, and the fractionation by the TSR process in high $\delta^{34}S$ values fluid needs further study.

There are two types of precipitation mechanisms of epigenetic celestine: (1) the mixture of Sr^{2+}-rich fluid and SO_4^{2-}-rich fluid, which causes the precipitation of celestine [21,27] and (2) the Sr^{2+}-rich fluid replaces gypsum or carbonate, forming celestine or strontianite [10]. Microthermometer studies of fluid inclusions in the celestine have not determined a fluid-mixing phenomenon. We conclude that the precipitation of celestine in Huayingshan is mainly related to the replacement of gypsum by Sr^{2+}-rich fluid, and the S of celestine dominantly derives from gypsum in the Jialingjiang Formation. The evidence supporting the above viewpoint is as follows: (1) the $\delta^{34}S$ values of celestine and gypsum from the Jialingjiang Formation are consistent in Huayingshan; (2) in situ analysis of celestine shows that there is a strong negative correlation between Sr and CaO ($R^2 = 0.95$), which may be the result of Sr replacing Ca in gypsum; (3) microscopic characteristics show clear evidence of epigenetic replacement of gypsum by celestine; (4) celestine orebodies occur in gypsum-rich members of the Jialingjiang Formation. The brines and hot springs in the eastern Sichuan Basin are rich with SO_4^{2-}, and evidence of $\delta^{34}S$ values indicates that these SO_4^{2-} originate from dissolved gypsum in the Jialingjiang Formation, suggesting that no obvious sulfur isotope fractionation occurred during the process of dissolving sulfate, which is the reason why the $\delta^{34}S$ values of celestine are consistent with that of gypsum.

6.3. Mechanism of Mineralization

Two hypotheses have been proposed for the genesis of celestine deposits: (1) celestine was formed during the evaporation of seawater [123,124] and (2) celestine was formed during the replacement of carbonates and gypsum by ore-forming fluid [3,21]. Moreover, it is also believed that some epigenetic celestine deposits are formed by fluid mixing, which refers to Sr^{2+}-rich fluid and SO_4^{2-}-rich fluid [22,93]. Zherebtsova et al. [103] questioned the hypothesis of the genesis of syngenetic precipitation through experiments; however, some viewpoints considered that certain celestine deposits were formed by syngenetic precipitation, such as the celestine deposit in the Arabian Gulf [27,124]. The carbonate, evaporite, and clastic rocks formed in an evaporation environment generally contain high strontium content, indicating that Sr can be enriched in the process of syngenetic deposition. Numerous large-scale celestine deposits are associated with hydrothermal activity [10], and the absence of hydrothermal activity is not conducive to the formation of industrial orebodies. The celestine deposit in Dafengshan, another extra-large celestine deposit in Qinghai Province, China, and the Arabian Gulf accord with the above viewpoint [27,28,125].

The genesis of the celestine deposit in Huayingshan has been discussed in many published papers, but the viewpoints are inconsistent. Three principal viewpoints have been proposed: (1) the celestine that forms the orebody is formed by syngenetic precipitation and epigenetic replacement [35]; (2) the celestine deposits in Huayingshan are formed by the evaporation of seawater [40]; and (3) the celestine orebodies are mainly formed by replacement gypsum with Sr-rich basinal brines [126]. The results of microthermometry and the published H-O isotopes values indicate that the formation of celestine deposits in Huayingshan is related to hot brine activity, and the structure of the ore supports this conclusion, especially the existence of the vein-like ore, which proves that the formation of the orebody is related to hydrothermal activity, and some structural features also support this view.

Based on the analysis of typical celestine deposits in the world in the present work, we conclude that the metallogenic model of the celestine deposits in Huayingshan is as follows: (1) in the Early Triassic, the eastern part of the Sichuan Basin was in the Sabkha environment. During the process of seawater evaporation, Sr was concentrated in biological carbonate rocks and aragonite, forming the source bed (Figure 14a). (2) The epigenetic replacement of gypsum by celestine. Aragonite–calcite conversion, dolomitization, and brine circulation concentrate the strontium in the formation of brines, forming Sr-rich fluid. Under the action of structural stress, the ore-forming fluid migrated along the faults and intraformational faulted zones and replaced gypsum to form Celestine (Figure 14b). The microthermometer results indicate that different types of ore are formed by the same fluid action, and that the type of ore is determined by the channel of fluid. The tectonic stress of ore-forming fluid migration is related to regional folding, and the mechanism is the same as that of the celestine deposits in Abolfares and Likak, Iran [2,3]. (3) The supergene period is characterized by the dissolution of the orebody by meteoric water, especially at the turning point of the anticline, resulting in the discontinuity of the orebody [14] (Figure 14c). In addition to dissolution, strontianitzation occurs in the shallow part of the ore body under the effect of meteoric water [127]. The celestine deposits and occurrences in the Huayingshan Sr metallogenic belt have a similar geological background, so the celestine deposits in the metallogenic belt should have a similar metallogenic model, and the characteristics of different celestine deposits may have little difference.

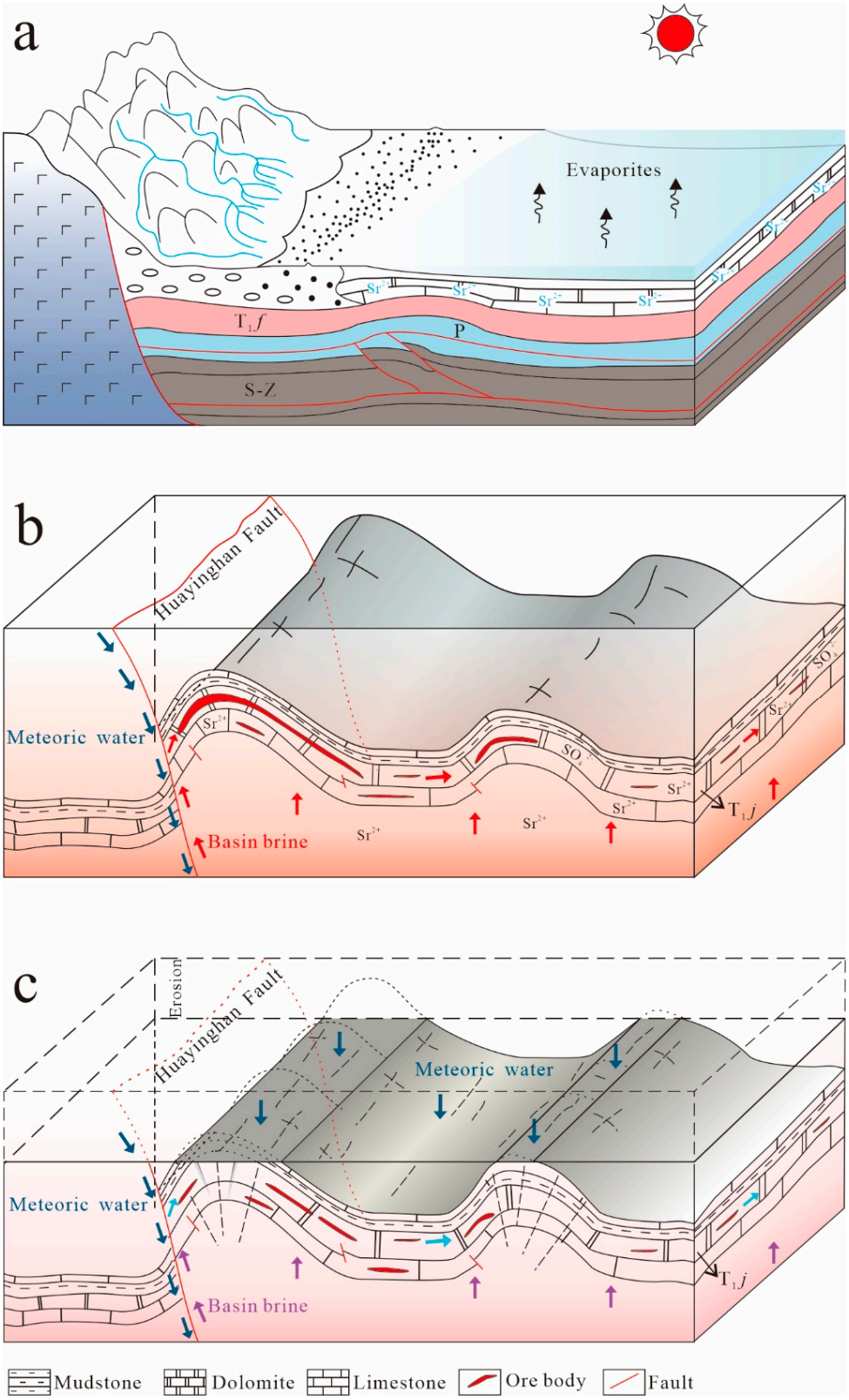

Figure 14. Metallogenic model for the celestine deposits in the Huayingshan area. (**a**) sr is enriched in carbonate rocks during the evaporation of seawater. (**b**) the brine in the basin replaced gypsum to form celestine during the migration process. (**c**) in the supergene stage, meteoric water dissolved part of the celestine ore bodies. The detailed description of subfigures (**a**–**c**) in the Section 6.3.

7. Conclusions

(1). Fluid inclusions of celestine in Huayingshan are mainly liquid-rich fluid inclusions, and the ore-forming fluids belong to the NaCl-H_2O system with medium–low temperature (190–220 °C) and low salinity (5–9 wt%, NaCl equiv.). The ore-forming fluids mainly drive from basinal brine, with the addition of a large amount of meteoric water. Different types of ore are formed by the same period of hydrothermal activity.

(2). The gas phase composition of the inclusions in the celestine is mainly CH_4, and these gases should drive from the destroyed paleo-hydrocarbon reservoirs within the Huayingshan ore district, which is different from other celestine deposits in the world.

(3). Strontium has many sources, but it predominantly derives from the Jialingjiang Formation, while the Sr in the Jialingjiang Formation derives from ancient seawater. The S in the celestine derives from gypsum in the Jialingjiang Formation. Sr and CaO showed a clear negative correlation, indicating that the precipitation of the celestine is caused by the replacement of gypsum with Sr-rich fluid.

(4). The genesis of the deposit belongs to the hydrothermal type related to basinal brines, and the ore-forming process is divided into the evaporation period, hydrothermal period, and supergene period.

Author Contributions: Writing—original draft preparation, Y.G.; sample collection, Y.S., D.W. and W.G.; methodology, Y.G., Y.S. and D.W.; figure drawing, B.C. and W.G.; writing—reviewing and editing, Y.S. All authors have read and agreed to the published version of the manuscript.

Funding: This work was supported by funds from the National Key R&D Program of China (2021YFC2901905), and China Geological Survey Project (DD20221695, DD20190379, DD20160346).

Data Availability Statement: Not applicable.

Acknowledgments: We are grateful for the assistance received during the preparation of this paper provided by Jianfeng Gao from the Institute of Geochemistry, Chinese Academy of Sciences.

Conflicts of Interest: The authors declare no conflict interest.

References

1. MacMillan, J.P.; Park, J.W.; Gerstenberg, R.; Wagner, H.; Köhler, K.; Wallbrecht, P. Strontium and Strontium Compounds. *Ullmann's Encycl. Ind. Chem.* **2000**, *34*, 473–480.
2. Ehya, F.; Shakouri, B.; Rafi, M. Geology, mineralogy, and isotope (Sr, S) geochemistry of the Likak celestite deposit, SW Iran. *Carbonates Evaporites* **2013**, *28*, 419–431. [CrossRef]
3. Pourkaseb, H.; Zarasvandi, A.; Rezaei, M.; Mahdavi, R.; Ghanavati, F. The occurrence and origin of celestite in the Abolfares region, Iran: Implications for Sr-mineralization in Zagros fold belt (ZFB). *J. Afr. Earth Sci.* **2017**, *134*, 352–364. [CrossRef]
4. Kile, D.E.; Dayvault, R.D.; Hood, W.C.; Hatch, H.S. Celestine-Bearing Geodes from Wayne and Emery Counties, Southeastern Utah: Genesis and Mineralogy. *Rocks Miner.* **2015**, *90*, 314–337. [CrossRef]
5. Souissi, F.; Sassi, R.; Dandurand, J.L.; Bouhlel, S.; Hamda, S.B. Fluid inclusion microthermometry and rare earth element distribution in the celestites of the jebel doghra ore deposit (dome zone, northern tunisia): Towards a new genetic model. *Bull. De La Soc. Geol. De Fr.* **2007**, *178*, 459–471. [CrossRef]
6. Wang, R.J.; Wang, D.H.; Li, J.K.; Sun, Y.; Li, D.X.; Guo, C.L.; Zhao, Z.; Yu, Y.; Huang, F.; Wang, C.H.; et al. *Three-Type Rare Mineral Resources (Rare Resources, Rare Earth and Rarely Scattered Resources) and Their Utilization*; Geological Publishing House: Beijing, China, 2015; p. 415. (In Chinese)
7. Fishburn, M.D.; Davis, J.C. Geology of the Celestite Deposits of Brown County, Kansas. *Trans. Kans. Acad. Sci. 1903* **1962**, *65*, 47–60. [CrossRef]
8. Baker, P.A.; Bloomer, S.H. The origin of celestite in deep-sea carbonate sediments. *Geochim. Et Cosmochim. Acta* **1988**, *52*, 335–339. [CrossRef]
9. Piga, G.; Marmi, J.; Galobart, À.; Brunetti, A.; Lasio, B.; Malfatti, L.; Enzo, S. New data on the presence of celestite into fossil bones from the uppermost Cretaceous Molí del Baró-1 site (Spain) and an alternative hypothesis on its origin. *Spectrochim. Acta Part B At. Spectrosc.* **2016**, *119*, 41–49. [CrossRef]
10. Hanor, J.S. A model for the origin of large carbonate-and evaporite-hosted celestine ($SrSO_4$) deposits. *J. Sediment. Res.* **2004**, *74*, 168–175. [CrossRef]
11. Hanor, J.S. Origin of saline fluids in sedimentary basins. *Geol. Soc. Lond. Spec. Publ.* **1994**, *78*, 151–174. [CrossRef]
12. Hanor, J.S. Barite-celestine geochemistry and environments of formation. *Rev. Mineral. Geochem.* **2000**, *40*, 193–275. [CrossRef]

13. Gu, W.S.; Li, J.; Huang, Z.Q.; Zhu, M.Z.; Tian, M. Analysis of metallogenic system of Yuxia-style Sr ore deposit. *China Min. Mag.* **2017**, *26*, 162–165. (In Chinese with English abstract)
14. Li, J.; Gu, W.S.; Huang, Z.Q.; Tian, M.; Zhu, M.Z.; Luo, Y.L.; Zhang, H. Study on supergenetic corrosion of Yuxia-style Sr ore deposit. *China Min. Mag.* **2017**, *26*, 154–160. (In Chinese with English abstract)
15. Xu, X.G.; Gao, Z.L.; Luo, Z.L.; Ma, Y.L. Discussion on genesis of Yuxia strontium deposit in Tongliang, Sichuan. *Acta Geol. Sichuan* **1990**, *10*, 259–266. (In Chinese)
16. Xu, X.G. Genetic types and prospecting direction of strontium deposits in China. *Geol. Chem. Miner.* **1991**, *1*, 20–28. (In Chinese)
17. Xu, X.G.; Gu, X.L. *Strontium Deposits in China*; Sichuan Science and Technology Press: Chengdu, China, 1999; p. 125. (In Chinese with English abstract)
18. García-Veigas, J.; Rosell, L.; Cendón, D.I.; Gibert, L.; Martín, J.M.; Torres-Ruiz, J.; Ortí, F. Large celestine orebodies formed by early-diagenetic replacement of gypsified stromatolites (Upper Miocene, Montevive–Escúzar deposit, Granada Basin, Spain). *Ore Geol. Rev.* **2015**, *64*, 187–199. [CrossRef]
19. Taberner, C.; Marshall, J.D.; Hendry, J.P.; Pierre, C.; Thirlwall, M.F. Celestite formation, bacterial sulphate reduction and carbonate cementation of Eocene reefs and basinal sediments (Igualada, NE Spain). *Sedimentology* **2002**, *49*, 171–190. [CrossRef]
20. Kesler, S.E.; Jones, L.M. Sulfur- and strontium-isotopic geochemistry of celestite, barite and gypsum from the Mesozoic basins of northeastern Mexico. *Chem. Geol.* **1981**, *31*, 211–224. [CrossRef]
21. Scholle, P.A.; Stemmerik, L.; Harpoth, O. Origin of major karst-associated celestite mineralization in Karstryggen, central East Greenland. *J. Sediment. Res.* **1990**, *60*, 397–410.
22. Abidi, R.; Slim-Shimi, N.; Marignac, C.; Hatira, N.; Gasquet, D.; Renac, C.; Soumarin, A.; Gleeson, S. The origin of sulfate mineralization and the nature of the $BaSO_4$–$SrSO_4$ solid-solution series in the Ain Allega and El Aguiba ore deposits, Northern Tunisia. *Ore Geol. Rev.* **2012**, *48*, 165–179. [CrossRef]
23. Brodtkorb, M.K.; Ramos, V.; Barbieri, M.; Ametrano, S. The evaporitic celestite-barite deposits of Neuquen, Argentina. *Miner. Depos.* **1982**, *17*, 423–436. [CrossRef]
24. Wood, M.W.; Shaw, H.F. The geochemistry of celestites from the Yate area near Bristol (U.K.). *Chem. Geol.* **1976**, *17*, 179–193. [CrossRef]
25. Carlson, E.H. Celestite replacements of evaporites in the Salina Group. *Sediment. Geol.* **1987**, *54*, 93–112. [CrossRef]
26. Tekin, E.; Varol, B.; Sayili, İ.S. Indications of intermediate compositions in the $BaSO_4$-$SrSO_4$ solid-solution series from Baheciktepe Celestine deposit, Sivas, east-central Anatolia, Turkey. *Can. Miner.* **2002**, *40*, 895–908. [CrossRef]
27. Dill, H.G.; Henjes-Kunst, F.; Berner, Z.; Stüben, D. Miocene diagenetic and epigenetic strontium mineralization in calcareous series from Cyprus and the Arabian Gulf: Metallogenic perspective on sub- and suprasalt redox-controlled base metal deposits. *J. Asian Earth Sci.* **2009**, *34*, 557–576. [CrossRef]
28. Sun, Y.; Liu, X.F.; Wang, R.J.; Chen, Z.Y.; Li, J.K.; Li, S.P.; Zhao, Z. Compositional characteristics of celestite in Dafengshan strontium deposit, Qinghai province. *Miner. Depos.* **2013**, *32*, 148–156. (In Chinese with English abstract)
29. Li, J. Discussion on the genesis of Hechuan strontium deposit. *Geol. Chem. Miner.* **1989**, *1*, 8–15. (In Chinese)
30. Li, J. Ore-forming geochemistry and formation mechanism of Hechuan celestite deposit. *China Nonmet. Miner. Ind. Nonmentallic Geol.* **1990**, *1*, 14–19+42+2. (In Chinese with English abstract)
31. Cheng, M. Comment on the underground hot brine genesis of the Yuxia strontium deposit in Tongliang, Sichuan. *Acta Geol. Sichuan* **1992**, *12*, 58–61. (In Chinese with English abstract)
32. Xu, Z.Z. The mechanism of tectonic control of Sr-ore belt, Huaying mountains, Sichuan. *J. Chengdu Univ. Technol.* **1994**, *21*, 79–86. (In Chinese with English abstract)
33. Qin, Z. Metallogenic characteristics of the celestite type Sr deposit in Chongqing area. *J. Chengdu Univ. Technol. Sci. Technol. Ed.* **1998**, *25*, 118–126. (In Chinese with English abstract)
34. Zhu, C.Y.; Wu, W.H. Stable isotopic characteristics and metallogenic mechanismof Huayingshan strontium mineralization belt. *Geochimica* **1999**, *2*, 197–202. (In Chinese with English abstract)
35. Wang, J.P.; Hu, M.T.; Zhou, J.M.; Zhu, J.B.; Deng, X.L.; Yang, Q.T. Two Origins of Celestite Ores in Huaying Mountains Area. *Acta Geol. Sin.* **2000**, *74*, 325–332+386. (In Chinese with English abstract)
36. Zhou, J.M.; Wang, J.P.; Yang, Q.T.; Zhu, J.B.; Deng, X.L.; Hu, M.T. Geochemical features of rare earth elements of celestite in Huaying mountains area. *Geol. Chem. Miner.* **2004**, *26*, 19–22. (In Chinese with English abstract)
37. Li, K.; Cai, C.; Jiang, L.; Cai, L.; Jia, L.; Zhang, B.; Xiang, L.; Yuan, Y. Sr evolution in the Upper Permian and Lower Triassic carbonates, northeast Sichuan basin, China: Constraints from chemistry, isotope and fluid inclusions. *Appl. Geochem.* **2012**, *27*, 2409–2424. [CrossRef]
38. Xu, C.H. *Brief Study on the Metallogenic Geological Setting and Genesis to Celestite Deposits in Mts. Huaying, Sichuan-Chongqing*; Chengdu University of Technology: Chengdu, China, 2016; pp. 1–74.
39. Hu, G.C. *Geological Characteristics and Discussion of Genesis to the Yuxia Celestite Mine in Tongliang of Chongqing*; Chengdu university of technology: Chengdu, China, 2017; pp. 1–78.
40. Song, W.Q.; Mao, X.D.; Xu, C.W. Characteristics of ore texture and structure of Yuxia celestite deposit in Chongqing and its genetic significance. *J. Chengdu Univ. Technol. Sci. Technol. Ed.* **2018**, *45*, 670–678. (In Chinese with English abstract)
41. Zhu, C.Y. The extraordinary enrichment of strontium element in the Yuxia large strontium deposit, Chongqing. *Bull. Mineral. Petrol. Geochem.* **1998**, *17*, 48–50. (In Chinese with English abstract)

42. Huang, S.J.; Lan, Y.F.; Huang, K.K.; Lü, J. Vug fillings and records of hydrothermal activity in the Middle Permian Qixia Formation, western Sichuan Basin. *Acta Petrol. Sin.* **2014**, *30*, 687–698. (In Chinese with English abstract)
43. Wang, E.; Meng, K.; Su, Z.; Meng, Q.R.; Chu, J.J.; Chen, Z.I.; Wang, G.; Shi, X.H.; Liang, X.Q. Block rotation: Tectonic response of the Sichuan basin to the southeastward growth of the Tibetan Plateau along the Xianshuihe-Xiaojiang fault. *Tectonics* **2014**, *33*, 686–718. [CrossRef]
44. Worley, B.A.; Wilson, C.J.L. Deformation partitioning and foliation reactivation during transpressional orogenesis, an example from the Central Longmen Shan, China. *J. Struct. Geol.* **1996**, *18*, 395–411. [CrossRef]
45. Li, J.; Xie, Z.; Dai, J.; Zhang, S.; Zhu, G.; Liu, Z. Geochemistry and origin of sour gas accumulations in the northeastern Sichuan Basin, SW China. *Org. Geochem.* **2005**, *36*, 1703–1716. [CrossRef]
46. Chen, S.F.; Wilson, C.J.L.; Worley, B.A. Tectonic transition from the Songpan-Garze Fold Belt to the Sichuan Basin, South-Western China. *Basin Res.* **1995**, *7*, 235–253. [CrossRef]
47. Burchfiel, B.C.; Chen, Z.; Liu, Y.; Royden, L.H. Tectonics of the Longmen Shan and Adjacent Regions, Central China. *Int. Geol. Rev.* **1995**, *37*, 661–735. [CrossRef]
48. Wen, Z.J.; Liang, J.T.; Ke, M.Y.; Gui, M.W.; Zhi, Z.L. Segmentation of the Longmen Mountains thrust belt, Western Sichuan Foreland Basin, SW China. *Tectonophysics* **2010**, *485*, 107–121.
49. Zhu, M.; Chen, H.L.; Zhou, J.; Yang, S.F. Provenance change from the Middle to Late Triassic of the southwestern Sichuan basin, Southwest China: Constraints from the sedimentary record and its tectonic significance. *Tectonophysics* **2017**, *700–701*, 92–107. [CrossRef]
50. Li, Y.Q.; He, D.F.; Chen, L.B.; Mei, Q.H.; Li, C.X.; Zhang, L. Cretaceous sedimentary basins in Sichuan, SW China: Restoration of tectonic and depositional environments. *Cretac. Res.* **2016**, *57*, 50–65. [CrossRef]
51. Shen, C.B.; Mei, L.F.; Xu, S.H. Fission track dating of mesozoic sandstones and its tectonic significance in the Eastern Sichuan Basin, China. *Radiat. Meas.* **2009**, *44*, 945–949. [CrossRef]
52. Shi, H.C.; Shi, X.B.; Glasmacher, U.A.; Yang, X.Q.; Stockli, D.F. The evolution of eastern Sichuan basin, Yangtze block since Cretaceous: Constraints from low temperature thermochronology. *J. Asian Earth Sci.* **2016**, *116*, 208–221. [CrossRef]
53. Zhang, Y.Q.; Dong, S.W.; Li, J.H.; Shi, W. Mesozoic multi-directional compressional tectonics and formation-reformation of Sichuan basin. *Geol. China* **2011**, *38*, 233–250, (In Chinese with English abstract).
54. Li, J.H.; Zhang, Y.Q.; Zhao, G.C.; Johnston, S.T.; Dong, S.W.; Koppers, A.; Miggins, D.P.; Sun, H.S.; Wang, W.B.; Xin, Y.J. New insights into Phanerozoic tectonics of South China: Early Paleozoic sinistral and Triassic dextral transpression in the east Wuyishan and Chencai domains, NE Cathaysia. *Tectonics* **2017**, *36*, 819–853. [CrossRef]
55. Jia, X.L. *Structural Geometry and Kinematics of Southeast Sichuan Basin: Insights into Tectonic Relationship with the Western Segment of Xue Feng Mountain Orogenic Belt*; China University of Geosciences (Beijing): Beijing, China, 2016; p. 262.
56. Zhuang, X.G.; Su, S.C.; Xiao, M.G.; Li, J.; Alastuey, A.; Querol, X. Mineralogy and geochemistry of the late permian coals in the Huayingshan coal-bearing area, Sichuan Province China. *Int. J. Coal Geol.* **2012**, *94*, 271–282. [CrossRef]
57. Zhou, Q.Y.; Shao, L.Y.; Chen, Z.X.; Li, M.B.; Yan, H.; Li, Y.J.; Chen, Z.S. Depositional environments and coal-accumulation characteristics of the Upper Triassic Xujiahe Formation in the northern segment of Huaying Mountain, Sichuan Basin. *J. China Coal Soc.* **2016**, *41*, 703–711. (In Chinese with English abstract)
58. Dai, S.F.; Luo, Y.B.; Seredin, V.V.; Ward, C.R.; Hower, J.C.; Zhao, L.; Liu, S.D.; Zhao, C.L.; Tianhe, M.; Zou, J.H. Revisiting the late Permian coal from the Huayingshan, Sichuan, southwestern China: Enrichment and occurrence modes of minerals and trace elements. *Int. J. Coal Geol.* **2014**, *22*, 110–128. [CrossRef]
59. Liu, S.; Ren, X.G.; Yao, S.X.; Liu, Z.P.; Ning, M.; Wang, X.; Huang, X.H. Relationship between gas reservoir distribution and structural system of upper Triassic Xujiahe Fm in the Sichuan. *Nat. Gas Ind. B* **2019**, *6*, 220–235. [CrossRef]
60. Yang, P.; Cheng, Q.; Xie, S.; Wang, J.; Chang, L.; Yu, Q.; Zhan, Z.; Chen, F. Hydrogeochemistry and geothermometry of deep thermal water in the carbonate formation in the main urban area of Chongqing, China. *J. Hydrol.* **2017**, *549*, 50–61. [CrossRef]
61. Ma, Y.; Zhang, S.; Guo, T.; Zhu, G.; Cai, X.; Li, M. Petroleum geology of the Puguang sour gas field in the Sichuan Basin, SW China. *Mar. Pet. Geol.* **2008**, *25*, 357–370. [CrossRef]
62. Liu, H.; Sun, Z.; Li, Z.P.; Li, L.; Nie, Y.; Wu, J.J.; Zhou, X.G.; Tan, X.C. Syndepositional tectonic activities in the Huayingshan fracture belt during the triassic Jialing river phase and its impact on sedimentation and reservoir development. *J. Stratigr.* **2010**, *34*, 312–320. (In Chinese with English abstract)
63. Wang, Z.J.; Wang, H.C.; Dong, D.; Qin, J. Review of Geophysical Results of Huayingshan Fault Zone. *Earthq. Res. Sichuan* **2018**, *3*, 6–12. (In Chinese with English abstract)
64. Xu, S.R.; Xu, J.H. The new results of seismic exploitation in Huayingshan fault zone. *Acta Pet. Sin.* **1986**, *7*, 39–48. (In Chinese with English abstract)
65. Ma, Y.S.; Mu, C.L.; Guo, T.L.; Tan, Q.Y.; Yu, Q. Sequence stratigraphy and reservoir distribution of Feixianguan formation in Northeastern Sichuan. *J. Mineral. Petrol.* **2005**, *25*, 73–79. (In Chinese with English abstract)
66. Chongqing Institute of Geology and mineral resources. *Investigation and Evaluation of Celestite Resources in Huayingshan Strontium Belt*; Chongqing Institute of Geology and Mineral Resources: Chongqing, China, 2015; pp. 1–62.
67. Jia, X.L.; He, D.F. Structural analysis and kinematics simulation of Xishan anticline in Southeast folded belt, Sichuan basin. *Xinjiang Pet. Geol.* **2014**, *35*, 652–658. (In Chinese with English abstract)

68. Bodnar, R.J. Revised equation and table for determining the freezing point depression of H_2O-NaCl solutions. *Geochim. Et Cosmochim. Acta* **1993**, *57*, 683–684. [CrossRef]
69. Liu, J.J.; Lü, Z.C.; Liu, Z.J.; Zhai, D.G.; Wang, Y.H.; Tao, Y.L. Strontium isotopic composition and its genetic significance of the Dabashan large barium metallogenic belt in southern Qinling Mountains. *Earth Sci. Front.* **2014**, *21*, 23–30. (In Chinese with English abstract)
70. Liu, Y.S.; Hu, Z.C.; Gao, S.; Günther, D.; Xu, J.; Gao, C.G.; Chen, H.H. In situ analysis of major and trace elements of anhydrous minerals by LA-ICP-MS without applying an internal standard. *Chem. Geol.* **2008**, *257*, 34–43. [CrossRef]
71. LI, J. Evaporite formation and celestine deposit. *Geol. Chem. Miner. Chem. Geol.* **1990**, 2, 15–21.
72. Huang, S.J.; Huang, Y.; Lan, Y.F.; Huang, K.K. A comparative study on strontium isotope composition of dolomites andtheir coeval seawater in the late permian-early Triassic, NE Sichuan basin. *Acta Petrol. Sin.* **2011**, *27*, 3831–3842. (In Chinese with English abstract)
73. Korte, C.; Kozur, H.W.; Bruckschen, P.; Veizer, J. Strontium isotope evolution of Late Permian and Triassic seawater. *Geochim. Et Cosmochim. Acta* **2003**, *67*, 47–62. [CrossRef]
74. Lin, Y.T. Study on sulfur isotopes of trias marine deposit gypsum and brines in the Sichuan basin. *J. Salt Lake Res.* **2003**, *11*, 1–7. (In Chinese with English abstract)
75. Zhong, Y.-J.; Chen, A.-Q.; Huang, K.-K.; Yang, S.; Xu, S.-L.; Somerville, I.D. Hydrothermal activity in the fourth member of the Triassic Leikoupo Formation in the Yuanba area, northeast Sichuan, SW China. *Geol. J.* **2019**, *54*, 266–277. [CrossRef]
76. Huang, K.K.; Zhong, Y.J.; Huang, S.J.; Li, X.N.; Feng, M.S. Saddle-dolomite-bearing fracture fillings and records of hot brine activity in the Jialingjiang formation, Libixia section, Hechuan area of Chongqing city. *Acta Geol. Sin.* **2016**, *90*, 195–208.
77. Tekin, E.; Varol, B.; Friedman, G.M. A prelimennary study Celestite-bearing gypsum in the Tertiary Sivas basin, central-eastern Turkey. *Carbonates Evaporites* **2001**, *16*, 93–101. [CrossRef]
78. Taherzadeh, A.; Paydar, G.R. Geology, Geochemistry and Origin of Baba Mohammad Celestite Deposit, Kohgiloyeh and Boyerahmad Province, Iran. In *8th Symposium of Iranian Society of Economic Geology*; Azimzadeh, D.m.A.M., Ed.; University of Zanjan: Zanjan, Iran, 2016.
79. Tekin, E.; Varol, B.; Ayan, Z.; Satir, M. Epigenetic origin of celestite deposits in the Tertiary Sivas Basin: New mineralogical and geochemical evidence. *Neues Jahrb. Für Mineral. Mon.* **2002**, *2002*, 289–318. [CrossRef]
80. Abidi, R.; Slim-Shimi, N.; Gasquet, D.; Hatira, N.; Somarin, A. Genesis of celestite—Bearing cap rock formation from the Ain Allega ore deposit (northern Tunisia): Contributions from microthermometric studies. *Bull. De La Société Géologique De Fr.* **2011**, *182*, 427–435. [CrossRef]
81. Jabal, A.; Akhdar, A.; Ne, L.; Saad, K.; El Ebaidi, S. Geochemical and mineralogical studies of the Celestite bearing formations and associated sediments in Benghazi Formation, Ar Rajmah Group (Middle Miocene) Al Jabal Al Akhdar, NE Libya. *Libyan J. Sci. Technol.* **2019**, *1*, 1.
82. Bazargani-Guilani, K.; Tak, M.A.N. Celestite ore deposit and occurrences of the Qom Formation, Oligo-Miocene, central Iran. In Proceedings of the 2nd IASME/WSEAS International Conference on GEOLOGY and SEISMOLOGY (GES '08), Cambridge, UK, 23–25 February 2008; pp. 48–54.
83. Zhou, X.; Li, C.J.; Ju, X.M.; Du, Q.; Tong, L.H. Origin of Subsurface Brines in the Sichuan Basin. *Ground Water* **1997**, *35*, 53–58.
84. Huang, S.J.; Hairuo, Q.; Hu, Z.W.; Zou, M.L.; Feng, W.L.; Wang, C.M.; Gao, X.Y.; Wang, Q.D. Influence of sulfate reduction on diagenesis of Feixianguan carbonate in Triassic, NE Sichuan basin of China. *Acta Sedimentol. Sin.* **2007**, *25*, 815–824. (In Chinese with English abstract)
85. Zhou, X.; Cao, Q.; Yin, F.; Guo, J.; Wang, X.C.; Zhang, Y.; Wang, L.; Shen, Y. Characteristics of the brines and hot springs in the Triassic carbonates in the high and steep fold zone of the eastern Sichuan basin. *Acta Geol. Sin.* **2015**, *89*, 1908–1920. (In Chinese with English abstract)
86. Li, K.K.; George, S.C.; Cai, C.F.; Gong, S.; Sestak, S.; Armand, S.; Zhang, X.F. Fluid inclusion and stable isotopic studies of thermochemical sulfate reduction: Upper permian and lower triassic gasfields, northeast Sichuan Basin, China. *Geochim. Et Cosmochim. Acta* **2019**, *246*, 86–108. [CrossRef]
87. Hao, F.; Zhang, X.F.; Wang, C.W.; Li, P.P.; Guo, T.L.; Zou, H.Y.; Zhu, Y.M.; Liu, J.Z.; Cai, Z.X. The fate of CO2 derived from thermochemical sulfate reduction (TSR) and effect of TSR on carbonate porosity and permeability, Sichuan Basin, China. *Earth Sci. Rev.* **2015**, *141*, 154–177. [CrossRef]
88. Cai, C.F.; Xiang, L.; Yuan, Y.Y.; Xu, C.L.; He, W.X.; Tang, Y.J.; Borjigin, T. Sulfur and carbon isotopic compositions of the Permian to Triassic TSR and non-TSR altered solid bitumen and its parent source rock in NE Sichuan Basin. *Org. Geochem.* **2017**, *105*, 1–12. [CrossRef]
89. Xu, X.G. Genetic types of celestite deposits and their prospecting direciton discussed from strontium geochemistry. *Geol. Rev.* **1984**, *30*, 146–154. (In Chinese with English abstract)
90. Cheng, Q.; Yang, H.L.; Zeng, M. The formation and protection of karst geothermal water resources in the main urban area of Chongqing. *Carsologica Sin.* **2015**, *34*, 217–227. (In Chinese with English abstract)
91. Playà, E.; Rosell, L. The celestite problem in gypsum Sr geochemistry: An evaluation of purifying methods of gypsiferous samples. *Chem. Geol.* **2005**, *221*, 102–116. [CrossRef]
92. Madsen, H.B.; Stemmerik, L. Early diagenetic celestite replacement of demosponges in Upper Cretaceous (Campanian–Maastrichtian) chalk, Stevns, Denmark. *Geology* **2009**, *37*, 355–358. [CrossRef]

93. Breesch, L.; Stemmerik, L. Genetic and fluid flow model of a large-scale celestite deposit in Karstryggen, Central East Greenland. *J. Geochem. Explor.* **2009**, *101*, 9. [CrossRef]
94. Mcarthur, J.M.; Burnett, J.; Hancock, J.M. Strontium isotopes at K/T boundary. *Nature* **1992**, *355*, 28. [CrossRef]
95. Burke, W.H.; Denison, R.E.; Hetherington, E.A.; Koepnick, R.B.; Nelson, H.F.; Otto, J.B. Variation of seawater 87Sr/86Sr throughout Phanerozoic time. *Geology* **1982**, *10*, 516. [CrossRef]
96. Huang, S.J.; Hairuo, Q.; Huang, P.P.; Huo, Z.W.; Wang, Q.D.; Zou, M.L.; Liu, H.N. Strontium isotopic composition and evolution of seawater from Late Permian to Early Triassic-Based on the Results of Marine Carbonate in Zhongliang Mountain, Chongqing. *Sci. China Earth Sci.* **2008**, *38*, 273–283. (In Chinese)
97. Veizer, J.; Ala, D.; Azmy, K.; Bruckschen, P.; Buhl, D.; Bruhn, F.; Carden, G.A.F.; Diener, A.; Ebneth, S.; Godderis, Y. $^{87}Sr/^{86}Sr$, $\delta^{13}C$ and $\delta^{18}O$ evolution of Phanerozoic seawater. *Chem. Geol.* **1999**, *161*, 1586. [CrossRef]
98. Prokoph, A.; Shields, G.A.; Veizer, J. Compilation and time-series analysis of a marine carbonate $\delta^{18}O$, $\delta^{13}C$, $^{87}Sr/^{86}Sr$ and $\delta^{34}S$ database through Earth history. *Earth Sci. Rev.* **2008**, *87*, 113–133. [CrossRef]
99. Joachimski, M.; Lai, X.L.; Shen, S.Z.; Jiang, H.; Luo, G.M.; Chen, B.; Chen, J.; Sun, Y.D. Climate warming in the latest Permian and the Permian-Triassic mass extinction. *Geology* **2012**, *40*, 195–198. [CrossRef]
100. Lin, L.B.; Chen, H.D.; Zhu, L.D.; Xu, S.L.; Zhong, Y.J. The sequence-based lithofacies-paleogeography of Jialingjiang Formation and Leikoupo Formation in eastern Sichuan Basin, China. *J. Chengdu Univ. Technol.* **2010**, *37*, 446–451. (In Chinese with English abstract)
101. Canfield, D.; Raiswell, R. Carbonate precipitation and dissolution. In *Taphonomy—Releasing the Data Locked in the Fossil Record*; Allison, A., Briggs, D.E.G., Eds.; Plenum Press: New York, NY, USA, 1991; pp. 411–453.
102. Wolf, K.H. Carbonate sediments and their diagenesis. *Earth Sci. Rev.* **1973**, *9*, 152–157. [CrossRef]
103. Zherebtsova, I.K.; Volkova, N.N. Experimental study of behavior of trace elements in the process of natural solar evaporation of Black Sea water and Sasyk-Sivash brine. *Geokhimiya* **1966**, *3*, 832–845.
104. Katz, A.; Sass, E.; Starinsky, A.; Holland, H.D. Strontium behavior in the aragonite-calcite transformation: An experimental study at 40–98 °C. *Geochim. Et Cosmochim. Acta* **1972**, *36*, 481–496. [CrossRef]
105. Helz, G.R.; Holland, H.D. The solubility and geologic occurrence of strontianite. *Geochim. Et Cosmochim. Acta* **1965**, *29*, 1303–1315. [CrossRef]
106. Sayles, F.L.; Manheim, F.T. Interstitial solutions and diagenesis in deeply buried marine sediments: Results from the Deep Sea Drilling Project. *Geochim. Et Cosmochim. Acta* **1975**, *39*, 103–127. [CrossRef]
107. Huang, S.J.; Qing, H.R.; Hu, Z.W.; Zou, M.L.; Feng, W.L.; Wang, C.M.; Gao, X.Y.; Wang, Q.D. Closed-system dolomitization and the significance for petroleum and economic geology: An example from Feixianguan carbonates, Triassic NE Sichuan basin of China. *Acta Geol. Sin.* **2007**, *23*, 2955–2962. (In Chinese with English abstract)
108. Poonoosamy, J.; Curti, E.; Kosakowski, G.; Grolimund, D.; Van Loon, L.R.; Mäder, U. Barite precipitation following celestite dissolution in a porous medium: A SEM/BSE and μ-XRD/XRF study. *Geochim. Et Cosmochim. Acta* **2016**, *182*, 131–144. [CrossRef]
109. Canfield, D.E. Isotope fractionation by natural populations of sulfate-reducing bacteria. *Geochim. Et Cosmochim. Acta* **2011**, *65*, 1117–1124. [CrossRef]
110. Chen, J.S.; Chu, X.L. Sulfur isotope composition of triassic marine sulfates of South China. *Chem. Geol. Isot. Geosci. Sect.* **1988**, *72*, 155–161.
111. Bottrell, S.H.; Newton, R.J. Reconstruction of changes in global sulfur cycling from marine sulfate isotopes. *Earth Sci. Rev.* **2006**, *75*, 59–83. [CrossRef]
112. Claypool, G.E.; Holser, W.T.; Kaplan, I.R.; Sakai, H.; Zak, I. The age curves of sulfur and oxygen isotopes in marine sulfate and their mutual interpretation. *Chem. Geol.* **1980**, *28*, 199–260. [CrossRef]
113. Henjes-Kunst, E.; Raith, J.G.; Boyce, A.J. Micro-scale sulfur isotope and chemical variations in sphalerite from the Bleiberg Pb-Zn deposit, Eastern Alps, Austria. *Ore Geol. Rev.* **2017**, *90*, 52–62. [CrossRef]
114. Fazli, S.; Taghipour, B.; Moore, F.; Lentz, D.R. Fluid inclusions, S isotopes, and Pb isotopes characteristics of the Kuh-e-Surmeh carbonate-hosted Zn–Pb deposit in the Zagros Fold Belt, southwest Iran: Implications for the source of metals and sulfur and MVT genetic model. *Ore Geol. Rev.* **2019**, *109*, 615–629. [CrossRef]
115. Yang, Q.; Liu, W.; Zhang, J.; Wang, J.; Zhang, X. Formation of Pb–Zn deposits in the Sichuan–Yunnan–Guizhou triangle linked to the Youjiang foreland basin: Evidence from Rb–Sr age and in situ sulfur isotope analysis of the Maoping Pb–Zn deposit in northeastern Yunnan Province, southeast China. *Ore Geol. Rev.* **2019**, *107*, 780–800. [CrossRef]
116. Sheng, X.; Bi, X.; Hu, R.; Tang, Y.; Lan, Q.; Xiao, J.; Tao, Y.; Huang, M.; Peng, J.; Xu, L. The mineralization process of the Lanuoma Pb-Zn-Sb deposit in the Sanjiang Tethys region: Constraints from in situ sulfur isotopes and trace element compositions. *Ore Geol. Rev.* **2019**, *111*, 102941. [CrossRef]
117. Yan, J.X.; Carlson, E.H. Nodular celestite in the Chihsia Formation (Middle Permian) of south China. *Sedimentology* **2003**, *50*, 265–278. [CrossRef]
118. Machel, H.G.; Krouse, H.R.; Sassen, R. Products and distinguishing criteria of bacterial and thermochemical sulfate reduction. *Appl. Geochem.* **1995**, *10*, 373–389. [CrossRef]
119. Machel, H.G. Bacterial and thermochemical sulfate reduction in diagenetic settings-old and new insights. *Sediment. Geol.* **2001**, *140*, 143–175. [CrossRef]

120. Cai, C.F.; Li, K.K.; Zhu, Y.M.; Xiang, L.; Jiang, L.; Cai, X.Y.; Cai, L.L. TSR origin of sulfur in Permian and Triassic reservoir bitumen, East Sichuan Basin, China. *Org. Geochem.* **2010**, *41*, 871–878. [CrossRef]
121. Zhu, G.Y.; Zhang, S.C.; Liang, Y.B.; Dai, J.X. Stable sulfur isotopic composition of hydrogen sulfide and its genesis in Sichuan basin. *Geochimica* **2006**, *35*, 333–345. (In Chinese with English abstract)
122. Cross, M.M.; Bottrell, S.H. Reconciling experimentally observed sulphur isotope fractionation during thermochemical sulphate reduction (TSR) with field data: A 'steadystate' model of isotopic behaviour. *Goldschmidt J. Conf. Abstr.* **2000**, *5*, 325.
123. Hryniv, S.; Peryt, T.M. Strontium distribution and celestite occurrence in Zechstein (Upper Permian) anhydrites of West Poland. *Chem. Der Erde Geochem.* **2010**, *70*, 137–147. [CrossRef]
124. Rosenberg, Y.O.; Sade, Z.; Ganor, J. The precipitation of gypsum, celestine, and barite and coprecipitation of radium during seawater evaporation. *Geochim. Et Cosmochim. Acta* **2018**, *233*, 50–65. [CrossRef]
125. Shi, H.Y.; Miao, W.L.; Zhang, X.Y.; Li, W.X.; Tang, Q.L.; Li, Y.S. Geochemical characteristics and ore-forming material source of celestite deposits in Dafeng mountain, Northwestern Qaidam basin. *Acta Geol. Sin.* **2018**, *92*, 1733–1752.
126. Shan, Y.W.; Xiao, Y.F.; Juan, H.J.; Zhang, J.; Xu, C.; Guo, X.Z.; Li, X.R. Characteristics and metallogenic conditions of the Huayingshan strontium belt in Southeastern Sichuan. *Geol. J. China Univ.* **2013**, *19*, 267–268. (In Chinese with English abstract)
127. Turianicova, E. CO_2 utilization for mechanochemical carbonation of celestine. *Geosci. Eng.* **2015**, *61*, 20–23. [CrossRef]

Disclaimer/Publisher's Note: The statements, opinions and data contained in all publications are solely those of the individual author(s) and contributor(s) and not of MDPI and/or the editor(s). MDPI and/or the editor(s) disclaim responsibility for any injury to people or property resulting from any ideas, methods, instructions or products referred to in the content.